Identification of FHL1 as a regulator of skeletal muscle mass: implications for human myopathy

Belinda S. Cowling,[1] Meagan J. McGrath,[1] Mai-Anh Nguyen,[3] Denny L. Cottle,[1] Anthony J. Kee,[3,4] Susan Brown,[1] Joachim Schessl,[2] Yaqun Zou,[2] Josephine Joya,[3] Carsten G. Bönnemann,[2] Edna C. Hardeman,[3,4] and Christina A. Mitchell[1]

[1]Department of Biochemistry and Molecular Biology, Monash University, Clayton 3800, Victoria, Australia
[2]Division of Neurology, the Children's Hospital of Philadelphia, Pennsylvania Muscle Institute, University of Pennsylvania School of Medicine, Philadelphia, PA 19104
[3]Muscle Development Unit, the Children's Medical Research Institute, Westmead, Sydney 2145, New South Wales, Australia
[4]School of Medical Sciences, the University of New South Wales, Sydney 2052, New South Wales, Australia

Regulators of skeletal muscle mass are of interest, given the morbidity and mortality of muscle atrophy and myopathy. Four-and-a-half LIM protein 1 (FHL1) is mutated in several human myopathies, including reducing-body myopathy (RBM). The normal function of FHL1 in muscle and how it causes myopathy remains unknown. We find that FHL1 transgenic expression in mouse skeletal muscle promotes hypertrophy and an oxidative fiber-type switch, leading to increased whole-body strength and fatigue resistance. Additionally, FHL1 overexpression enhances myoblast fusion, resulting in hypertrophic myotubes in C2C12 cells, (a phenotype rescued by calcineurin inhibition). In FHL1-RBM C2C12 cells, there are no hypertrophic myotubes. FHL1 binds with the calcineurin-regulated transcription factor NFATc1 (nuclear factor of activated T cells, cytoplasmic, calcineurin-dependent 1), enhancing NFATc1 transcriptional activity. Mutant RBM-FHL1 forms aggregate bodies in C2C12 cells, sequestering NFATc1 and resulting in reduced NFAT nuclear translocation and transcriptional activity. NFATc1 also co-localizes with mutant FHL1 to reducing bodies in RBM-afflicted skeletal muscle. Therefore, via NFATc1 signaling regulation, FHL1 appears to modulate muscle mass and strength enhancement.

Introduction

Skeletal muscle mass and fiber size is dynamically responsive to changes in workload that lead to increased muscle mass and strength. In contrast, muscle atrophy leads to significant weakness in many inflammatory and infectious diseases, cancer, and human aging. Myopathies are muscle disorders characterized by atrophy of skeletal muscle. Proteins that regulate muscle hypertrophy are much sought after as therapeutic targets for reducing the debilitating effects of muscle atrophy and myopathies (Patel and Muntoni, 2004).

Four-and-a-half LIM protein 1 (FHL1; also named SLIM1 or KyoT1) belongs to the FHL protein family that comprises four and a half Lin-11, Isl-1, and Mec-3 (LIM) domains. FHL LIM domains mediate protein–protein interactions, scaffolding signaling proteins in the cytoplasm, and transcription factors in the nucleus (McGrath et al., 2003, 2006; Cottle et al., 2007). Three FHLs are expressed in skeletal muscle: FHL1, -2, and -3. There are no reports of FHL2 or 3 functioning to regulate skeletal muscle mass; rather, FHL2 regulates bone density (Gunther et al., 2005), and in muscle cell lines, FHL3 inhibits differentiation (Cottle et al., 2007). FHL2 and 3 function as transcriptional corepressors and/or coactivators (Johannessen et al., 2006; Cottle et al., 2007); however, FHL1 transcriptional targets and function in skeletal muscle are largely uncharacterized. Several lines of evidence support an association between FHL1 expression and hypertrophy. FHL1 mRNA is up-regulated during embryonic skeletal muscle development (Loughna et al., 2000), increasing with postnatal skeletal muscle growth 10- to 15-fold, and also increasing two- to threefold in stretch-induced muscle hypertrophy (Morgan et al., 1995; Morgan and Madgwick, 1999;

Correspondence to Christina A. Mitchell: christina.mitchell@med.monash.edu.au

Abbreviations used in this paper: CsA, cyclosporine A; CSA, cross-sectional area; EDL, extensor digitorum longus; FDP, flexor digitorum profundus; FHL, four-and-a-half LIM protein; HSA, human skeletal muscle α-actin; LIM, Lin-11, Isl-1, Mec-3; MHC, myosin heavy chain; NBT, nitro blue tetrazolium chloride; NFAT, nuclear factor of activated T cells; RBM, reducing body myopathy.

The Rockefeller University Press $30.00
J. Cell Biol. Vol. 183 No. 6 1033–1048
www.jcb.org/cgi/doi/10.1083/jcb.200804077

Loughna et al., 2000). Conversely, FHL1 mRNA decreases during disuse-induced muscle atrophy (Loughna et al., 2000). However, whether FHL1 itself directly promotes skeletal muscle hypertrophy or whether FHL1 mRNA increases as a consequence of hypertrophy is unknown.

Recently, FHL1 mutations have been identified in three human myopathies, including an X-linked, recessive, adult-onset scapuloperoneal myopathy called XMPMA, which presents with postural muscle atrophy and a bent spine, with pseudohypertrophy of other muscles (Windpassinger et al., 2008); an X-linked dominant scapuloperoneal syndrome associated with muscle atrophy but no pseudohypertrophy (Quinzii et al., 2008); and third, the most severe myopathy, a sporadic or familial reducing body myopathy (RBM; Schessl et al., 2008). Clinical severity in RBM ranges from early childhood-onset muscle weakness followed rapidly by death caused by respiratory failure to adult-onset muscle weakness with slower but relentless progression (Brooke and Neville, 1972; Kiyomoto et al., 1995; Figarella-Branger et al., 1999; Liewluck et al., 2007). RBM muscle shows cytoplasmic inclusions (reducing bodies), which contain aggregates proposed to arise from the accumulation of misfolded proteins (Liewluck et al., 2007). The molecular mechanisms by which FHL1 mutations contribute to RBM or other myopathies remain unknown.

Here, we have investigated the role FHL1 plays in regulating postnatal skeletal muscle growth by generating transgenic mice that ectopically express FHL1 in skeletal muscle. These mice exhibit skeletal muscle hypertrophy, with increased whole-body strength. Regulation of calcineurin/nuclear factor of activated T cells (NFAT) signaling may benefit select types of muscular dystrophy (Chakkalakal et al., 2004; St-Pierre et al., 2004; Parsons et al., 2007). We identify NFATc1 as a transcriptional target of FHL1. Wild-type FHL1, but not FHL1 mutants associated with RBM, enhanced NFATc1 transcriptional activity. RBM mutant FHL1 sequestered NFATc1 to reducing-body aggregates, leading to its decreased nuclear translocation in response to calcineurin activation. Therefore, FHL1 functions to increase skeletal muscle mass, and its loss of function and/or misfolding in RBM may sequester and trap its transcriptional targets to reducing-body aggregates. These studies identify FHL1 as a potential therapeutic target for increasing skeletal muscle mass in human myopathies.

Results

FHL1 promotes myoblast fusion and myotube hypertrophy

Differentiation of skeletal myoblasts (myogenesis) is defined by an ordered series of events (Abmayr et al., 2003). After induction of differentiation, myoblasts withdraw from the cell cycle, then elongate, align, and fuse to form primary multinucleated myotubes. A second wave of myoblast fusion results in further myonuclei addition to nascent myotubes, followed by the assembly of myofibrillar proteins into the costamere and sarcomere (Sanger et al., 2002). We have previously demonstrated that FHL1 promotes myoblast elongation in Sol8 myoblast cell lines (McGrath et al., 2003) and is important for sarcomere formation (McGrath et al., 2006). To investigate the role FHL1 plays in myoblast fusion and differentiation, C2C12 skeletal myoblasts were transiently transfected with HA-FHL1 or HA-βgal control and induced to differentiate to myotubes. Overexpression of FHL1 resulted in the formation of large "sac-like" myotubes containing dense clusters of nuclei (Fig. 1, C and D, arrows), in contrast to the thin, elongated myotubes containing a linear arrangement of myonuclei observed in HA-βgal control cells (Fig. 1, A and B). Analysis of myotube diameters revealed a shift toward larger myotubes, with FHL1 overexpression resulting in ∼20% of myotubes being >40 μm in diameter, compared with only 5% of control myotubes (see Fig. 7 B).

The large, sac-like myotube phenotype induced by FHL1 is reminiscent of myotube hypertrophy (Palmer et al., 2001; Rommel et al., 2001; Pisconti et al., 2006; Marshall et al., 2008), including hypertrophy caused by activation of the calcineurin–NFAT pathway by insulin-like growth factor 1 (IGF-1; Musarò et al., 1999; Musarò and Rosenthal, 1999; Semsarian et al., 1999a). To determine if FHL1 promoted myotube hypertrophy via the calcineurin–NFAT pathway, HA-FHL1–expressing myoblasts were treated with the calcineurin inhibitor cyclosporine A (CsA) at the onset and throughout the course of differentiation (Fig. 1, E and F). CsA inhibits the differentiation of primary muscle cultures and some muscle cell lines (Musarò et al., 1999; Delling et al., 2000; Friday et al., 2000); however, differentiation of the C2C12 myoblast cell line is totally resistant to CsA (Palmer et al., 2001). Indeed, CsA did not impede differentiation of HA-βgal control-expressing myotubes (Fig. 1 E). This allowed us to uniquely assess whether FHL1-induced myotube hypertrophy was dependent on calcineurin–NFAT signaling, uncomplicated by the effects of CsA on myoblast differentiation by itself. Interestingly, CsA prevented FHL1-induced hypertrophic myotube formation (Fig. 1 F), which suggests that FHL1 may promote myotube hypertrophy via regulation of the calcineurin–NFAT pathway.

Skeletal muscle hypertrophy is characterized by enhanced transcription/translation leading to increased protein synthesis, predominantly of myofibrillar proteins, which may be coupled with reduced protein breakdown (Furmanczyk and Quinn, 2003; Boonyarom and Inui, 2006). Concomitant with increased protein synthesis, and perhaps a feature of more advanced hypertrophy (Sandri, 2008), is activation and fusion of quiescent myoblasts called satellite cells with each other or with existing myofibers, resulting in myonuclei addition (Adams, 2006; O'Connor and Pavlath, 2007). We next evaluated whether FHL1-induced myotube hypertrophy was a consequence of enhanced myoblast fusion and/or differentiation and if this was accompanied by increased protein synthesis. Myoblasts stably expressing HA-FHL1 or HA-βgal control generated as described previously (McGrath et al., 2006) were induced to differentiate for 0–96 h and stained with markers of myoblast differentiation, myogenin and sarcomeric myosin heavy chain (MHC; Fig. 2 A; Cottle et al., 2007). Differentiation was assessed by scoring the percentage of myogenin-positive nuclei, which revealed a twofold increase in HA-FHL1–expressing cells, but only after 96 h differentiation (Fig. 2 B). The differentiation index represents the proportion of nuclei that are localized within MHC-positive myotubes and is used as a measure of

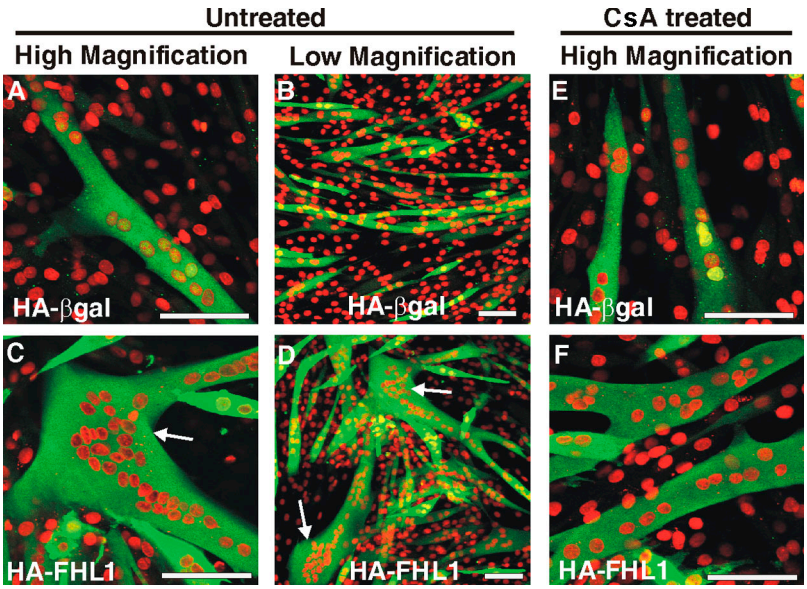

Figure 1. **FHL1 induces formation of hypertrophic myotubes, dependent upon calcineurin signaling.** C2C12 myoblasts were transiently transfected with HA-βgal control (A, B, and E) or HA-FHL1 (C, D, and F), and left untreated (A–D) or treated with the calcineurin inhibitor CsA (E and F) before and during induction of differentiation in low serum media for 96 h. Transfected cells were detected using an HA antibody (green) and costained with propidium iodide (red) to identify nuclei. Cells were visualized using laser scanning confocal microscopy. Arrows indicate hypertrophic myotubes. Bars, 100 μm.

myoblast differentiation (Sabourin et al., 1999; Erbay et al., 2003). Normally, this does not exceed ~50% (Yoshida et al., 1998). HA-FHL1 myotubes exhibited a similar differentiation index to HA-βgal myotubes up until 72 h, but then increased approximately twofold at 96 h (Fig. 2 C). Myoblast fusion was scored as total nuclei per MHC-positive myotube (Sabourin et al., 1999). After a 96-h differentiation, HA-FHL1 cell lines showed enhanced cell fusion (Fig. 2 D). Therefore, FHL1 may promote myoblast fusion. We detected no changes in the levels or temporal appearance of the muscle regulatory factors MyoD, Myf5, or myogenin in FHL1-expressing cells during differentiation (Fig. 2 E). However, a fivefold increase in MHC expression was detected in FHL1-expressing cells at 48 h of differentiation (Fig. 2, E and F). Expression of MHC is induced during the latter stages of myoblast differentiation (Cole et al., 1993); however, accretion of this major myofibrillar protein is also indicative of muscle anabolism and hypertrophy (Furmanczyk and Quinn, 2003). Analysis of the protein/DNA ratios in FHL1-expressing myotubes compared with controls revealed a twofold increase in protein synthesis relative to DNA, a feature of skeletal muscle hypertrophy (Fig. 2 G; De Arcangelis et al., 2005). These studies reveal that FHL1 increases the fusion of myoblasts. The increased protein/DNA ratio coupled with evidence of MHC accretion may be indicative of myotube hypertrophy. An imbalance in the nuclear/cytoplasmic ratio caused by hyperfusion may lead to an increase in protein translation, which increases the myotube cytoplasmic volume (Adams, 2006; O'Connor and Pavlath, 2007).

FHL1 induces skeletal muscle hypertrophy and increased strength

We next investigated whether FHL1 expression in postmitotic myofibers induced skeletal muscle hypertrophy in vivo. The FHL1 cDNA was fused to an HA tag (HA-FHL1) and linked to the human skeletal muscle α-actin (HSA) promoter (Fig. 3 A), which drives skeletal muscle–specific expression (Brennan and Hardeman, 1993). Skeletal α-actin is expressed only after myoblast fusion to form myotubes, and expression persists in adult muscle (Cox et al., 1990) in the elongated postmitotic cells of the somites, as well as in adult mature myofibers, but not satellite cells (Gunning et al., 1987; Miniou et al., 1999; Shen et al., 2003). FHL1 transgenic mice were generated and two lines were characterized. Transgenic HA-FHL1 expression was restricted to skeletal muscle, most prominent in fast-twitch enriched muscles including gastrocnemius (Fig. 3, B and C, GAS), extensor digitorum longus (EDL), plantaris, extensor carpi ulnaris (ECU), and flexor digitorum profundus (FDP), which is consistent with HSA promoter activity (Tinsley et al., 1996), with no expression in other tissues (Fig. 3 D). FHL1 transgenic sarcomere structure appeared undisturbed, with normal α-actinin localization at the Z-line (Fig. S1, A and B, available at http://www.jcb.org/cgi/content/full/jcb.200804077/DC1). HA-FHL1 colocalized with endogenous FHL1 at the I-band (Fig. 3 E; McGrath et al., 2006).

FHL1 transgenic gastrocnemius muscle exhibited a significant increase in the total fiber cross-sectional area (CSA) at both 6 (1.2-fold; Fig. 4, A and B) and 12 weeks of age (not depicted). Analysis of gastrocnemius fiber diameters revealed an increase in the frequency of larger fibers (≥50 μm) in transgenic mice (Fig. 4 C). Myofibrils from FHL1 transgenic mice were significantly wider (1.3-fold) than the wild type (Fig. S1 C; Rosenblatt and Woods, 1992). Therefore, FHL1 induces skeletal muscle hypertrophy in vivo. Skeletal muscle hypertrophy can be accompanied by a fiber type conversion (Dunn et al., 1999), identified by scoring MHC isoform expression. A 10% increase in oxidative type 2A, MHC-positive fibers was detected in FHL1 transgenic FDP muscle, with a corresponding decrease in 2X fibers; however, this latter trend was not statistically significant (Fig. 4 D). No difference was detected in the frequency of type 2B (Fig. 4 D) or type 1 fibers in FHL1 transgenic FDP muscle (not depicted); however, the FDP is composed of <1% of type 1 fibers. Therefore, FHL1 promotes skeletal muscle hypertrophy associated with a switch toward oxidative fiber type expression.

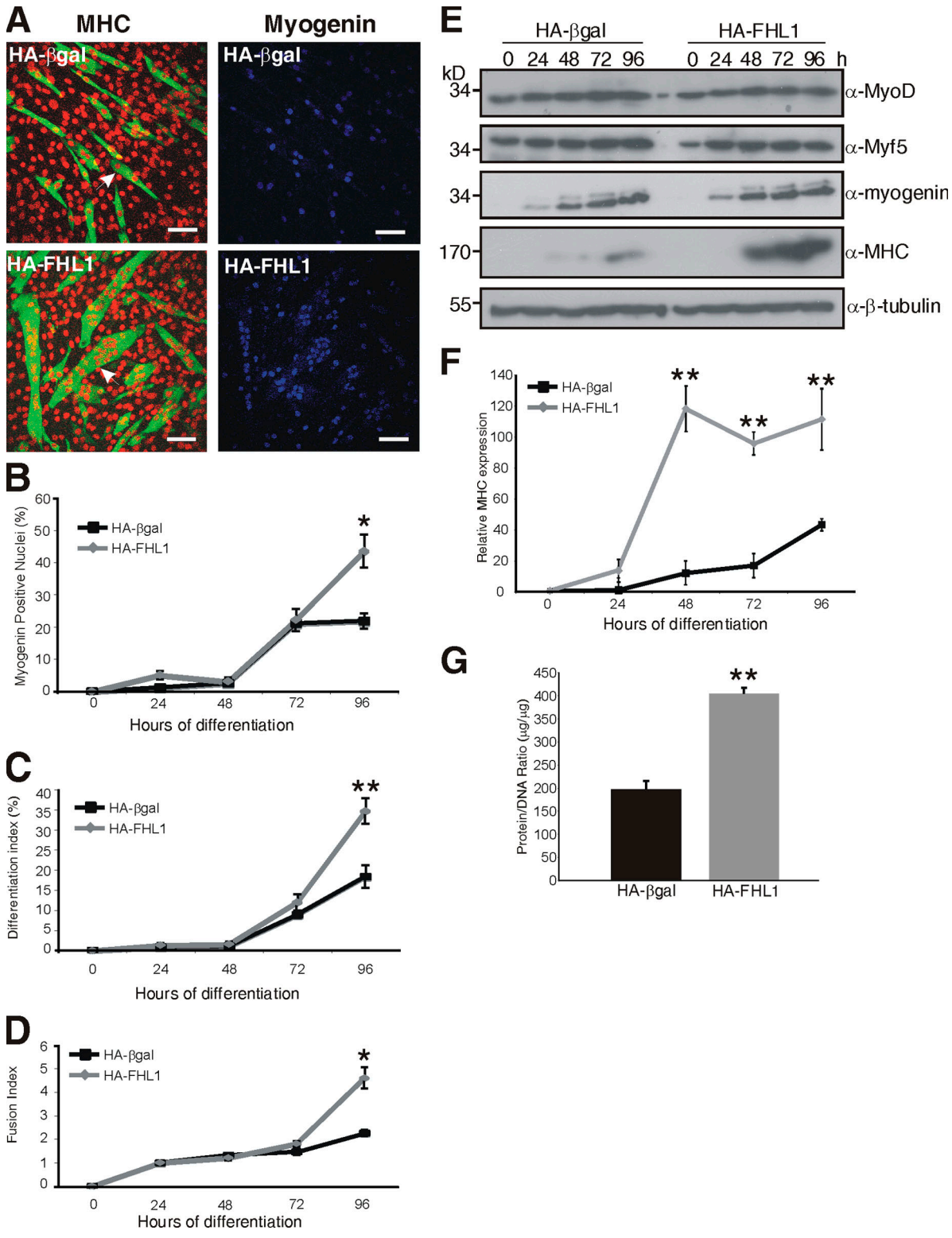

Figure 2. **FHL1 promotes enhanced myocyte fusion.** (A) C2C12 myoblasts stably expressing HA-βgal or HA-FHL1 were differentiated and costained with anti-MHC (MF20, green), myogenin antibodies (blue), and propidium iodide (red). Cells were imaged using confocal microscopy. Shown are representative images after 96 h of differentiation. Myoblast differentiation was quantified from 0–96 h. Arrows indicate examples of transfected myotubes. Bar, 70 μm. (B) The percentage of total nuclei positive for myogenin. (C) The differentiation index, determined by scoring the proportion of total nuclei within MHC-positive cells (myocytes and myotubes). (D) The fusion index, the mean number of nuclei per MHC-positive cell. Black and gray lines represent HA-βgal control and HA-FHL1–expressing C2C12 cells, respectively. Data represent the mean from three independent experiments (n = 3) ± SEM in which ≥100 cells were counted for each replicate. (*, $P < 0.05$; **, $P < 0.01$). (E) Lysates (25 μg) from differentiating C2C12 cells stably expressing HA-βgal or HA-FHL1 were immunoblotted with MyoD, Myf5, myogenin, MHC, and β-tubulin antibodies (loading control). (F) MHC expression was analyzed by densitometry and quantified relative to β-tubulin. Data represent the mean from three independent experiments ± SEM (n = 3; **, $P < 0.01$). (G) The DNA/protein ratio was determined. Data represent the mean from four independent experiments ± SEM (n = 4; **, $P < 0.01$).

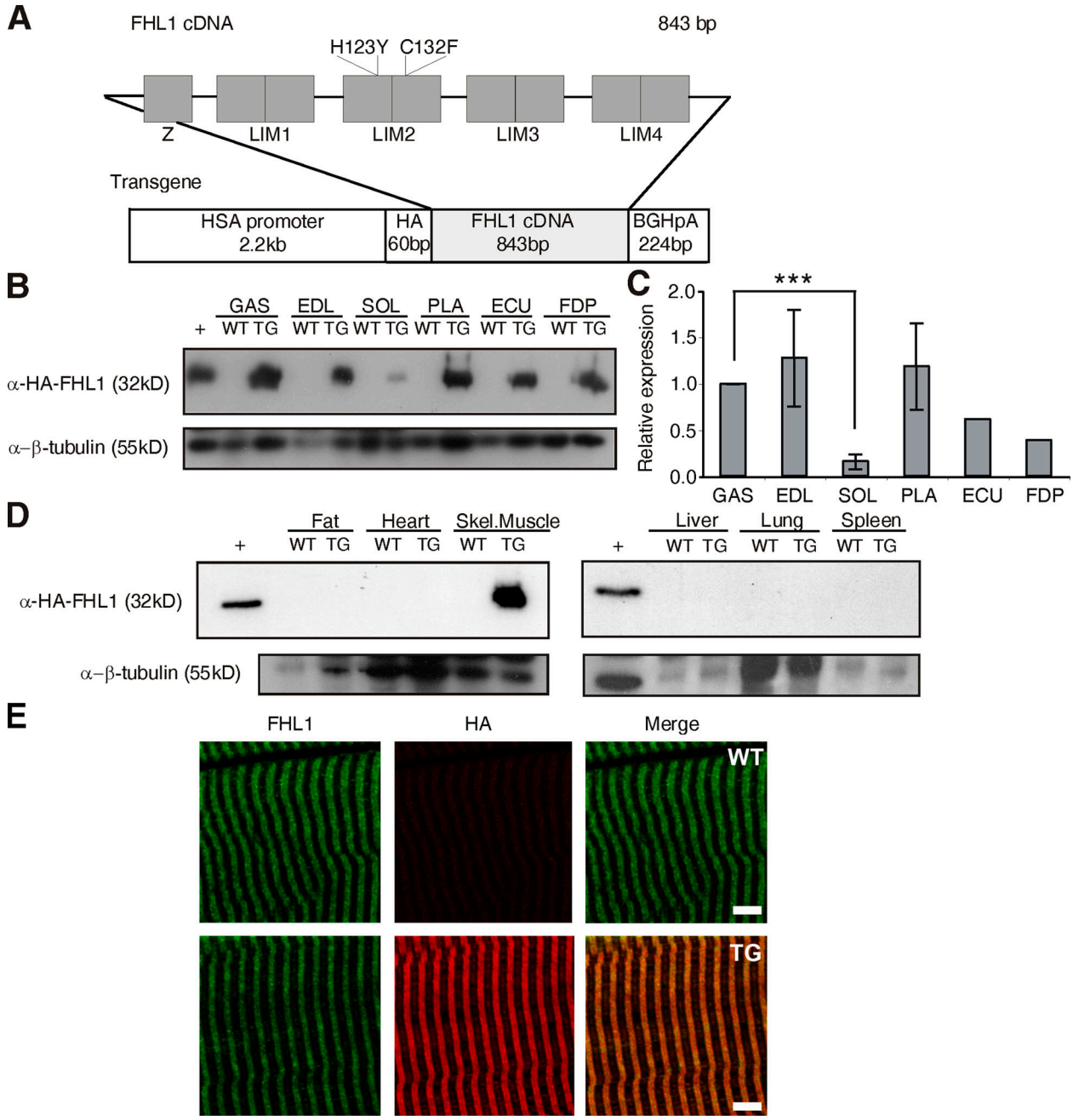

Figure 3. **Generation of FHL1 transgenic mice.** (A) The linearized transgene contains the 2.2-kb HSA promoter, fused in frame to the human FHL1 coding sequence with an N-terminal HA tag and a C-terminal bovine growth hormone polyA tail (BGHpA). FHL1-RBM mutants C132F and H123Y are indicated. (B) Skeletal muscle lysates were immunoblotted for HA-FHL1 or β-tubulin in wild-type (WT) or FHL1 transgenic (TG) muscle (GAS, gastrocnemius; EDL, extensor digitorum longus; SOL, soleus plantaris; PLA, plantaris; ECU, extensor carpi ulnaris; FDP, flexor digitorum profundus). A lysate prepared from C2C12 cells transfected with HA-FHL1 was used as a positive control (+). (C) The relative expression of HA-FHL1 was determined by densitometry of HA-immunoreactive polypeptides, standardized relative to β-tubulin loading. HA-FHL1 expression is represented as a fold difference, relative to GAS, arbitrarily defined as one. Graph depicts mean ± SEM (GAS, EDL, SOL, and PLA: $n = 3$ mice; ECU and FDP: ***, $P < 0.005$; $n = 1$ mouse). (D) Tissue lysates from WT or TG mice were immunoblotted for HA-FHL1 using anti-HA antibodies or β-tubulin. Lysates prepared from C2C12 cells transfected with HA-FHL1 were used as a positive control (+). (E) Longitudinal gastrocnemius muscle sections from WT or FHL-TG mice were stained with anti-FHL1 (green) or anti-HA (red) antibodies and imaged by confocal microscopy, then images were further resolved by deconvolution. Bars, 5 μm.

Analysis specifically of type 2B fiber diameters, which were expressed at equivalent frequencies in both FHL1 transgenic and wild-type mice (Fig. 4 D), identified an increase in the frequency of larger (≥50 μm) fibers, with a corresponding decrease in smaller (≤30 μm) fibers in both the FDP (Fig. 4, E and F) and EDL muscle (Fig. S2, available at http://www.jcb.org/cgi/content/full/jcb.200804077/DC1). The total number of fibers in the FDP and EDL muscles was not altered (unpublished data). Therefore, the skeletal muscle hypertrophy observed in FHL1 transgenic mice is caused by an increase in the muscle fiber size, rather than hyperplasia, or an increase in frequency of naturally occurring larger (type 2B) fibers.

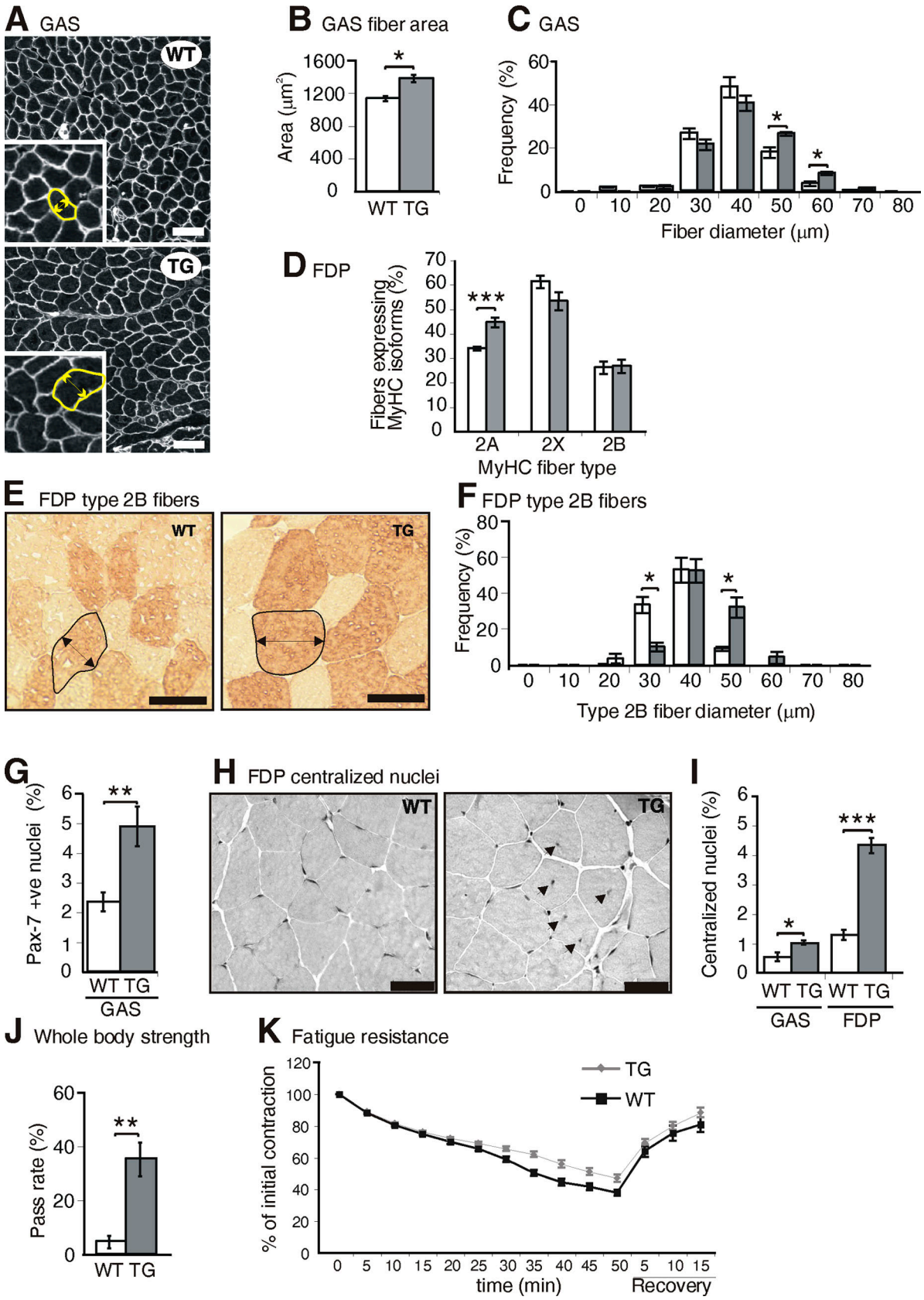

Figure 4. **FHL1 transgenic mice exhibit skeletal muscle hypertrophy, increased strength, and fatigue resistance.** (A) Transverse gastrocnemius sections were stained with a dystrophin antibody and viewed by confocal microscopy. Higher-magnification images are shown in the insets, with one fiber outlined. Bars, 50 μm. Images were analyzed for fiber area (B) and diameter (C; n = 3–4 mice; *, $P < 0.05$). GAS, gastrocnemius. (D) Transverse FDP sections were stained with MHC isoform-specific antibodies, and the percentage of 2A, 2X, and 2B fibers was calculated. The bar graph displays the frequency of each fiber type in wild-type (WT) versus transgenic (TG) mice (n = 3–5 mice; ***, $P < 0.005$). (E) Transverse FDP sections were stained for 2B MHC

Typically, the nuclei in adult muscle fibers reside at the fiber periphery. Nuclei located at the center of the fiber reflect satellite cell fusion with existing myofibers. A 2.1-fold increase in Pax-7 (a satellite cell marker)-positive nuclei (Fig. 4 G) and an increase in the number of centralized nuclei were detected in FHL1 transgenic mice at 6 and/or 12 wk, in both gastrocnemius (1.8-fold) and FDP (3.3-fold) muscles (Fig. 4, H and I). Satellite cells may be activated in both compensatory hypertrophy and extreme hypertrophy. The FHL1 transgene was expressed using the HSA promoter, which is active in muscle fibers in the mouse but not in satellite cells (Gunning et al., 1987; Miniou et al., 1999; Shen et al., 2003). Therefore, the increase in satellite cells in FHL1 transgenic muscle must be caused by a stimulatory effect of FHL1 overexpression in myofibers.

Next, we determined whether FHL1-induced skeletal muscle hypertrophy could enhance muscle strength. A standard whole-body strength test was performed, which measures overall strength of the limb and abdominal muscles (Joya et al., 2004). 12-wk-old mice were initially evaluated; however, all mice showed a 100% pass rate. Significantly, mature (12-mo old) FHL1 transgenic mice exhibited a 7.4-fold increase in whole-body strength relative to wild-type mice (Fig. 4 J), which indicates that FHL1 expression can enhance skeletal muscle strength in mature mice.

The muscle contractile properties of the EDL (Table S1, available at http://www.jcb.org/cgi/content/full/jcb.200804077/DC1) and soleus (not depicted) were examined but showed no difference between FHL1 transgenic versus wild-type mice for twitch or tetanic force when normalized to the CSA. Also, the rate of force production or relaxation was unaltered, perhaps because of the increased type 2A fibers (Fig. 4 D), which are slow to relax. Therefore, the increased whole-body strength exhibited by transgenic mice is a consequence of muscle hypertrophy and not increased myosin power stroke. In addition, greater fatigue resistance was detected in EDL transgenic muscle (Fig. 4 K), which exhibited skeletal muscle hypertrophy (Fig. S2). This may be caused by the increase in oxidative type 2A fibers observed in FHL1 transgenic mice (Fig. 4 D). In the soleus muscle, no difference was detected (unpublished data). However, the soleus showed low HA-FHL1 expression (Fig. 3, B and C) and did not exhibit hypertrophy (not depicted). Therefore, FHL1 induces skeletal muscle hypertrophy, increased muscle strength, and decreased susceptibility to fatigue.

Wild-type FHL1 binds NFATc1, and FHL1 RBM-associated mutants demonstrate reduced NFATc1 binding

The FHL proteins play critical roles as transcriptional coactivators or repressors (Johannessen et al., 2006; Cottle et al., 2007). Calcineurin signaling is implicated in regulating myopathy-related muscle degeneration, positively in some myopathies and negatively in others (Chakkalakal et al., 2004; St-Pierre et al., 2004; Parsons et al., 2007). Calcineurin is a calmodulin-dependent, calcium-activated protein phosphatase. Once activated, calcineurin dephosphorylates cytosolic NFAT transcription factors, exposing a nuclear localization sequence and thereby promoting their nuclear translocation and transcriptional events. NFATc1-c3 and NFAT5 are expressed in skeletal muscle (Abbott et al., 1998; O'Connor et al., 2007). NFATc1 promotes skeletal muscle hypertrophy and oxidative myofiber-type identity (Chin et al., 1998; Semsarian et al., 1999b), NFATc2 governs myofiber number (Horsley et al., 2001), and NFATc3 regulates primary myotube formation during myogenesis (Kegley et al., 2001). NFAT5 is a constitutively nuclear, calcineurin-independent transcription factor, which regulates skeletal muscle cell migration and differentiation (O'Connor et al., 2007). As FHL1 promoted hypertrophy and fiber type switching in vivo, which is reminiscent of NFATc1 function, we evaluated whether FHL1 interacted with NFATc1. GST-FHL1 bound His-NFATc1 in purified component binding studies (Fig. 5 A). In control studies, GST–GATA-2 complexed with His-NFATc1 as described previously (Musarò et al., 1999). Also, GST-FHL1, but not GST-coupled glutathione-Sepharose, incubated with skeletal muscle lysate pulled down an ~100-kD polypeptide that corresponds to endogenous NFATc1 (Fig. 5 B). We next asked whether FHL1-RBM mutants could also complex with NFATc1. C2C12 myoblasts were cotransfected with myc-NFATc1 and HA-FHL1 (wild type), HA-FHL1^{C132F}, or HA-FHL1^{H123Y}. HA-FHL1 was detected in myc-NFATc1 immunoprecipitates (Fig. 5 C). In contrast, binding of RBM-FHL1 mutants to myc-NFATc1, although evident (Fig. 5 C), was reduced by ~80% (Fig. 5 D). Mutant FHL1 is sequestered to reducing body aggregates in the skeletal muscle of RBM-affected individuals (Schessl et al., 2008). Therefore, the RBM mutant FHL1–NFATc1 complex may be less accessible for immunoprecipitation because of its sequestration in reducing body aggregates. To investigate this possibility, we examined the effect of wild-type or RBM mutant FHL1 on the subcellular localization of NFATc1; the latter has been found to localize to the myotube cytosol, and in response to calcineurin activation, in some but not all nuclei (Abbott et al., 1998). In differentiated C2C12 cells, wild-type HA-FHL1 and myc-NFATc1 colocalized in the cytosol (Fig. 6 A). FHL1^{C132F} and FHL1^{H123Y} localized diffusely in the cytosol but also in perinuclear cytoplasmic aggregates (Fig. 6 A, white arrowheads), which stained with the reducing body marker menadione–nitro blue tetrazolium chloride (NBT) in the absence of substrate (Fig. 6 A, black arrowheads), consistent with

fibers; one fiber is outlined per image. Bars, 40 µm. (F) The diameters of FDP-2B fibers from WT versus TG mice are shown (n = 3–4 mice; *, $P < 0.05$). (G) The frequency of Pax-7–positive nuclei in the gastrocnemius was scored, relative to total nuclei. The bar graph represents the frequency of Pax-7–positive nuclei for WT and TG mice (n = 3–5 mice; **, $P < 0.01$). (H) Transverse FDP sections were hematoxylin and eosin stained. Arrows indicate centralized nuclei. Bars, 40 µm. (I) The frequency of centralized nuclei were scored, relative to total myofiber nuclei, in transverse gastrocnemius and FDP sections (n = 4–6 mice; *, $P < 0.05$; ***, $P < 0.001$). (J) A whole animal strength test measured overall limb and abdominal strength as a percentage pass rate over 15 trials for WT versus TG 12-mo-old mice (n = 4–8; **, $P < 0.01$). All graphs represent mean ± SEM; WT, white; TG, gray. (K) Muscle fatigability was assessed as a drop in force with repeated tetanic contractions in EDL muscles from WT (black) versus TG (red) mice, expressed as a percentage of initial contraction over time, mean ± SEM (n = 7, $P < 0.02$).

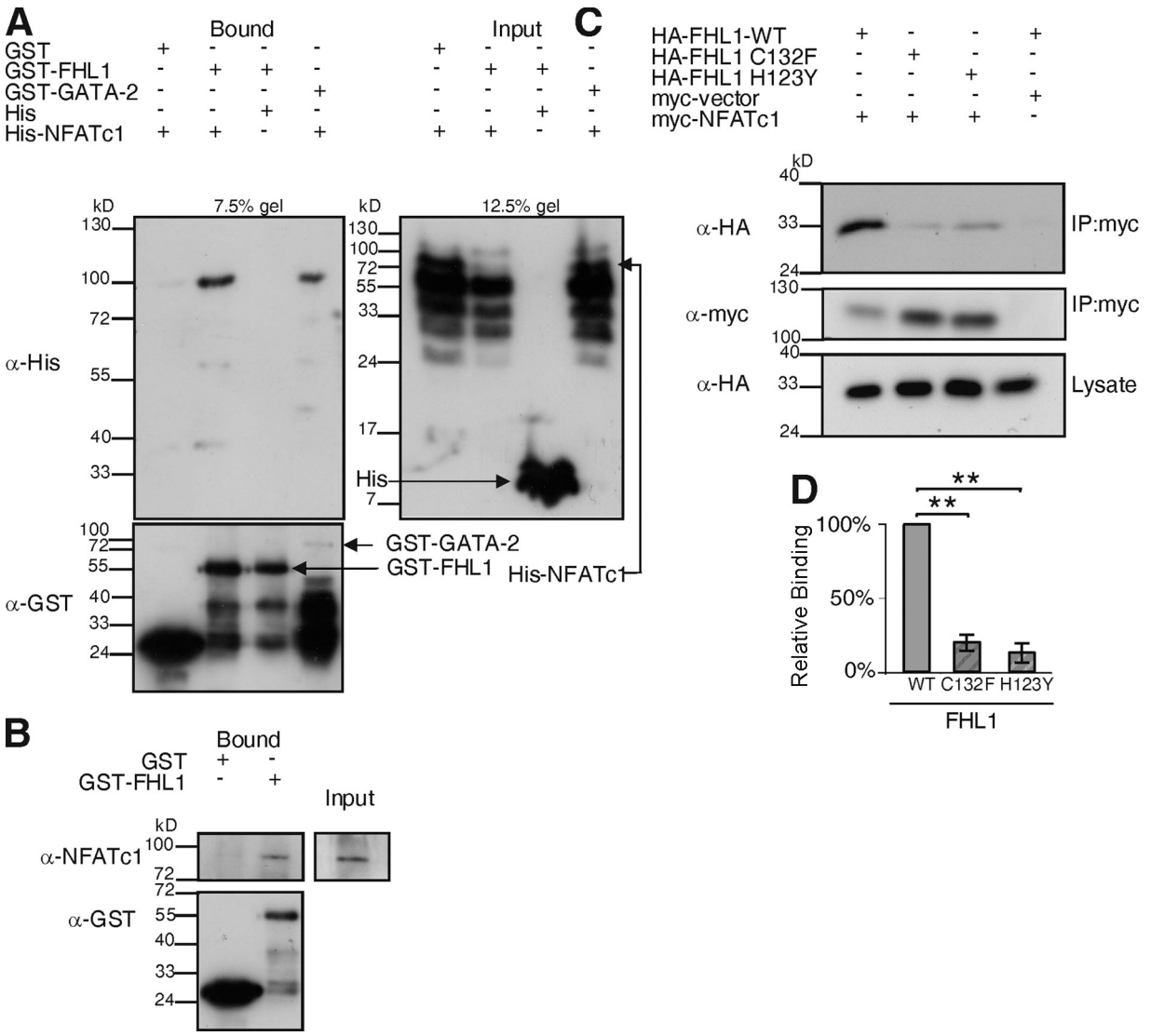

Figure 5. **FHL1 forms a complex with NFATc1.** (A) GST-FHL1, GST-GATA-2, or GST and His-NFATc1 or His were coexpressed as indicated in *E. coli*. GST proteins and associated proteins were bound to glutathione-Sepharose. Western blots are representative of three experiments. Arrows indicate GST- and His-tagged proteins. The His tag alone did not copurify with GST-FHL1 (not depicted). (B) GST-FHL1 or GST coupled to glutathione-Sepharose was incubated with skeletal muscle lysates from wild-type FVB/n mice and immunoblotted for endogenous NFATc1, GST, or GST-FHL1 as indicated. Results shown are representative of four similar experiments. (C) Coimmunoprecipitation of HA-FHL1 and myc-NFATc1 in C2C12 cells. C2C12 cells were transfected with the indicated constructs and immunoprecipitated with a myc antibody, then immunoblotted with an HA antibody (top). Immunoprecipitation of myc-NFATc1 was confirmed by immunoblotting with myc antibody (middle). Lysates were immunoblotted with an HA antibody to confirm equal expression of FHL1 constructs (bottom). Immunoblots are representative of three experiments. (D) Densitometric quantification of HA-FHL1 wild-type or C132F/H123Y mutants, relative to immunoprecipitated myc-NFAT. The bar graph represents the mean ± SEM (n = 3 experiments; **, $P < 0.01$).

reducing-body aggregates in RBM skeletal muscle (Schessl et al., 2008). Interestingly, NFATc1, when coexpressed with HA-FHL1^{C132F} or HA-FHL1^{H123Y} but not wild-type FHL1, also localized to reducing body aggregates (Fig. 6 A, insets). We obtained muscle biopsies from individuals with RBM and examined NFATc1 localization, revealing its reducing body aggregate colocalization with FHL1 (Fig. 6 B, arrowheads). We also determined the affect of FHL1-RBM mutants on NFATc1 nuclear translocation in response to the Ca^{2+} ionophore, ionomycin, which activates calcineurin signaling (Abbott et al., 1998). NFATc1 nuclear translocation was detected in 35% of myotube nuclei scored after ionomycin pretreatment, and this localization was not affected by FHL1 coexpression (Fig. 6, C and D). In contrast, NFATc1 nuclear localization was significantly reduced by HA-FHL1^{C132F} or HA-FHL1^{H123Y} coexpression, revealing that RBM-FHL1 mutants may sequester NFATc1 to reducing bodies and therefore reduce NFATc1 activity in the nucleus.

Wild-type FHL1, but not RBM-associated FHL1 mutants, coactivate NFATc1-mediated transcription

FHL1 mutations have been identified in patients with RBM that occur in critical residues within the second LIM domain (C132F or H123Y) and have been predicted to disrupt folding of the LIM domain, and, therefore, impair protein binding (Fig. 3 A;

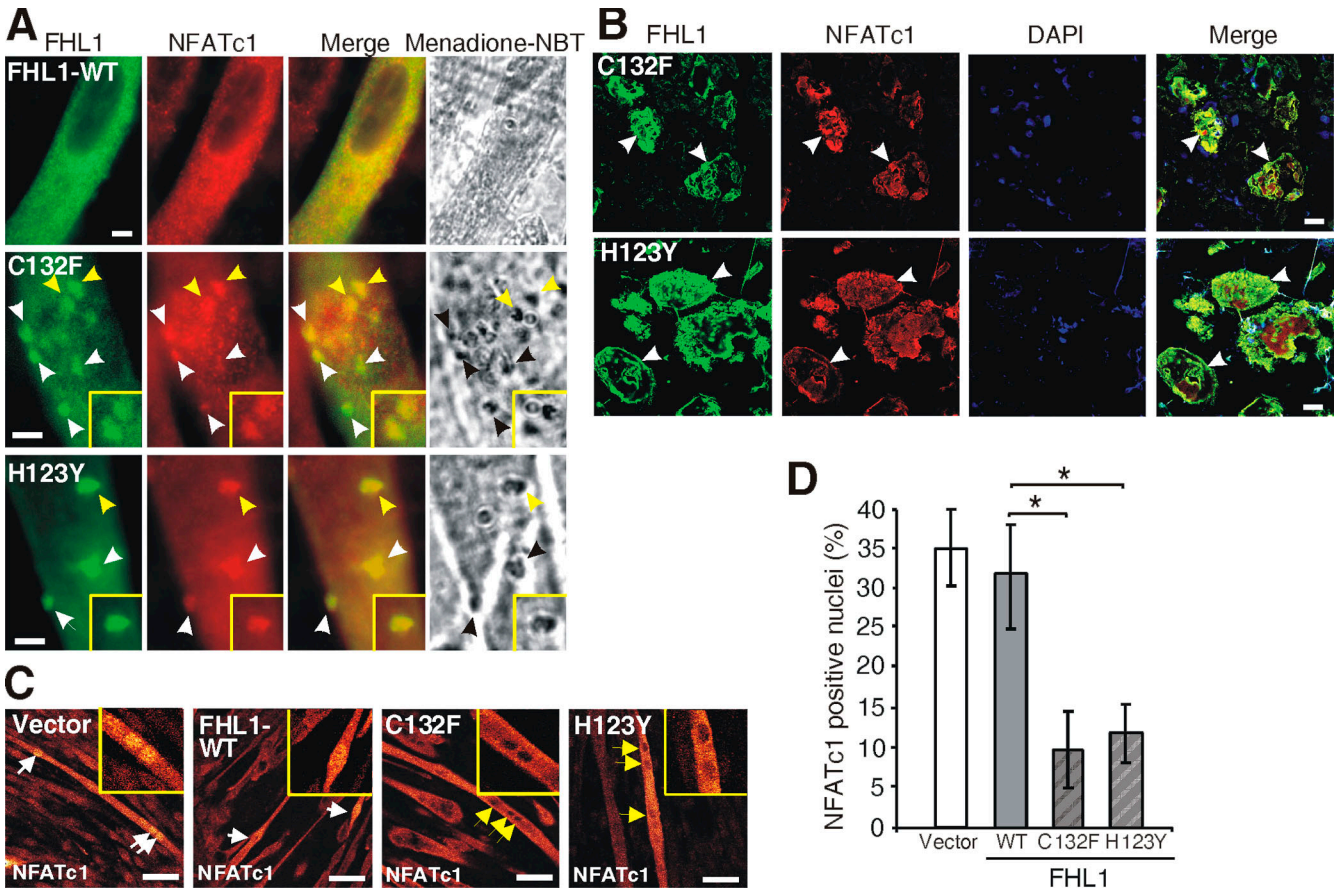

Figure 6. **RBM-FHL1 mutations alter localization of NFATc1.** (A) C2C12 myoblasts were cotransfected with HA-FHL1 wild-type (top), HA-FHL1^{C132F} (middle), or HA-FHL1^{H123Y} (bottom), and myc-NFATc1, then differentiated for 72 h. Myotubes were fixed and costained with HA (green) and myc (red) antibodies, costained with menadione-NBT, and imaged by fluorescence microscopy. White arrowheads indicate perinuclear aggregates colocalizing with the reducing-body marker menadione-NBT in the absence of substrate (black arrowheads). Yellow arrowheads reveal the region shown in the high-magnification images showing colocalization between FHL1, NFATc1, and menadione-NBT in the insets. (B) Transverse skeletal muscle sections were prepared from human RBM muscle biopsies, with FHL^{C132F} (top) or FHL1^{H123Y} (bottom) mutations. Sections were stained with antibodies recognizing FHL1 (green) and NFATc1 (red), then costained with DAPI (nuclei). Arrowheads identify reducing bodies. (C) Vector control, FHL1 wild-type (FHL1-WT), or indicated FHL1 RBM mutants were cotransfected with myc-NFATc1 into C2C12 myoblasts. Myoblasts were differentiated for 72 h, then ionomycin-stimulated for 30 min, and costained with anti-myc (NFATc1, glow-over images are shown) and anti-HA (to identify cotransfected cells, not depicted here). White arrows identify NFATc1 nuclear staining, yellow arrows indicate NFATc1-negative nuclei. High-magnification images are shown in the insets. (D) The percentage of transfected cells containing nuclear NFATc1 was scored after ionomycin stimulation. The bar graph equals mean ± SEM (n = 4 experiments; *, $P < 0.05$). Bars: (A and B) 20 µm; (C) 50 µm.

Schessl et al., 2008). To examine the functional consequence of these mutations, C2C12 myoblasts were transiently transfected with HA-FHL1^{C132F} or HA-FHL1^{H123Y}, then induced to differentiate, stained with an anti-HA antibody, and imaged using confocal microscopy (Fig. 7 A). In control studies, myoblasts were transiently transfected with wild-type HA-FHL1 (HA-FHL1-WT; Fig. 7 A). As described earlier (Fig. 1), overexpression of wild-type FHL1 induced the expression of large hypertrophic myotubes. Interestingly, FHL1^{C132F} did not induce formation of hypertrophic myotubes (Fig. 7 A), which suggests loss of FHL1 function. In addition, C2C12 myotubes expressing FHL1^{C132F} exhibited an approximately twofold increase in the frequency of smaller diameter (≤20 µm) myotubes (Fig. 7 B), which is reminiscent of the cell culture equivalent of muscle atrophy (Stevenson et al., 2005). Expression of FHL1^{H123Y}, a mutation associated with a milder clinical phenotype, also induced hypertrophic myotubes; however, the majority of cells differentiated normally (Fig. 7, A and B). In control studies, immunoblot analysis confirmed equal expression of wild-type and mutant FHL1 (unpublished data). Therefore, FHL1, but not mutant FHL1 associated with severe RBM, induces hypertrophic myotubes, a phenotype that we have demonstrated is dependent on calcineurin signaling.

We next investigated whether FHL1 binding to NFATc1 regulates NFATc1-dependent transcription. NFATc1 binds the IL-2 promoter, an NFAT-responsive gene in striated muscle (Ichida and Finkel, 2001). For C2C12 myoblasts grown in serum (growth conditions), the basal IL-2 reporter activity in vector-control cells was increased approximately threefold by coexpression of NFATc1, and further transactivated approximately ninefold by FHL1 (Fig. 7 C). FHL1^{C132F} and FHL1^{H123Y} exhibited reduced ability to transactivate NFAT-mediated IL-2 promoter reporter activity. Similarly, after myoblast differentiation, wild-type FHL1 but not RBM-FHL mutants transactivated NFATc1 reporter activity (Fig. 7 D). To determine if this transcriptional activation occurred in vivo, we examined for expression

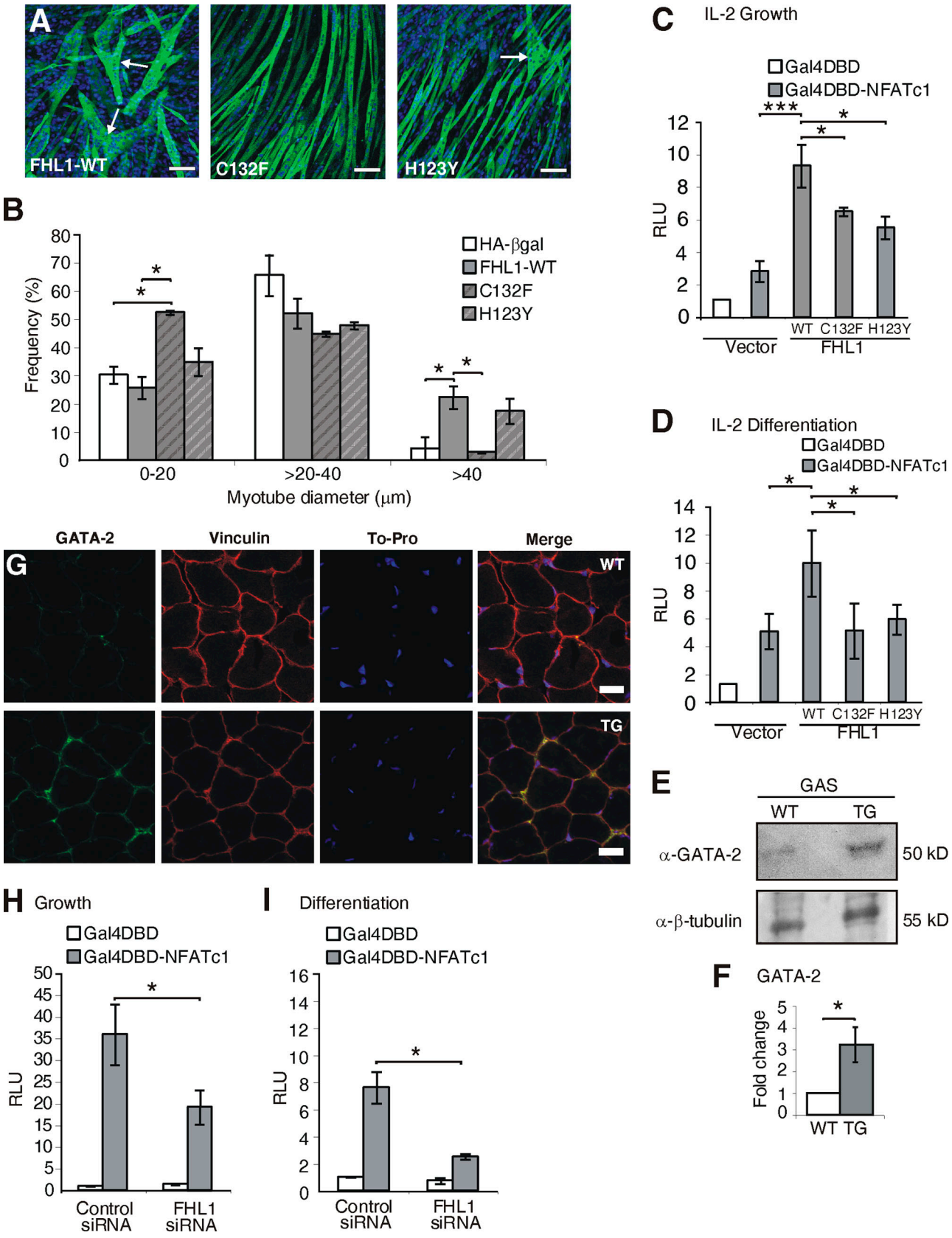

Figure 7. **FHL1 regulates the transcriptional activity of NFATc1 and expression of the calcineurin-responsive gene GATA-2.** (A) C2C12 myoblasts were transiently transfected with HA-tagged wild-type (WT) FHL1, FHL1^{C132F}, or FHL1^{H123Y} and allowed to differentiate for 72 h, then costained with anti-HA antibody (green) and To-Pro-3 (blue) to detect nuclei. Cells were imaged using confocal microscopy. Arrows indicate hypertrophic myotubes. Bars, 100 μm. (B) Maximum myotube diameter was measured in myotubes transiently transfected with HA-tagged wild-type (WT) FHL1, FHL1^{C132F}, FHL1^{H123Y}, or HA-βgal control, then differentiated for 96 h and stained as described in Materials and methods. The bar graph represents the mean frequency of myotubes with diameters of

of a calcineurin-responsive gene, GATA-2 (Musarò et al., 1999), in transgenic muscle. Although not normally expressed in skeletal muscle, GATA-2 expression is induced in hypertrophic skeletal muscle, where, despite being a transcription factor, it localizes to the sarcolemma (Paul and Rosenthal, 2002). Significantly, increased GATA-2 was detected in the gastrocnemius of FHL1 transgenic mice (Fig. 7 E, F). Furthermore, in FHL1 transgenic mice, increased GATA-2 was detected at the sarcolemma (Fig. 7 G).

To verify that FHL1 regulates NFATc1 transcriptional activity, the IL-2 promoter luciferase assay was repeated in C2C12 cells under conditions of siRNA-mediated FHL1 knockdown, as described previously (McGrath et al., 2006). Under growth conditions, FHL1 knockdown reduced NFATc1-dependent gene transcription ~1.8-fold relative to the siRNA scrambled (control) sequence (Fig. 7 H) and threefold under differentiation conditions (Fig. 7 I). FHL1 immunoblot analysis confirmed FHL1 protein knockdown under growth and differentiation conditions (Fig. S3, available at http://www.jcb.org/cgi/content/full/jcb.200804077/DC1). Therefore, FHL1 is required for efficient NFATc1-mediated transcriptional activity.

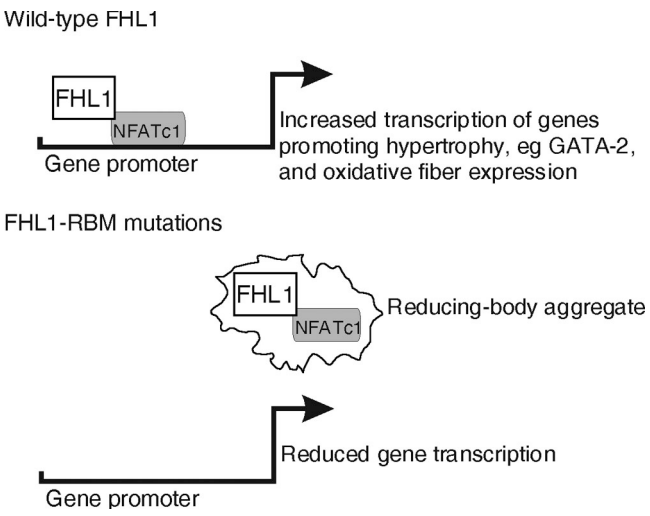

Figure 8. **FHL1 regulates NFAT-mediated signaling in skeletal muscle.** Wild-type FHL1 complexes with NFATc1 to increase its transcriptional activity, promoting skeletal muscle hypertrophy and oxidative fiber type expression. FHL1-RBM mutations sequester NFATc1 into reducing body aggregates, resulting in its reduced nuclear translocation and reduced activation of gene transcription.

Discussion

FHL1 has recently been identified as the gene mutated in several familial and sporadic human myopathies (Quinzii et al., 2008; Schessl et al., 2008; Windpassinger et al., 2008). However, the normal function of FHL1 in skeletal muscle and its molecular targets are largely uncharacterized. The discovery that FHL1 expression increases muscle fiber size and oxidative slow fiber type expression, leading to increased muscle strength and endurance, identifies it as a regulator of skeletal muscle mass. FHL1 complexes with NFATc1, thereby enhancing its transcriptional activity. In contrast, mutant FHL1 proteins that cause RBM sequestered NFATc1 to reducing body aggregates, resulting in decreased NFATc1 nuclear translocation and transcriptional activity. Collectively, the data presented here provide evidence for a role for FHL1 in regulating skeletal muscle mass via regulation of NFATc1 transcriptional activity (Fig. 8).

FHL1 transgenic mice exhibited skeletal muscle hypertrophy rather than hyperplasia, showing a ~20% increase in fiber size but no change in fiber number. However, this was insufficient to increase overall muscle weight relative to body weight (unpublished data). The increase in muscle fiber size in FHL1 transgenic mice induced an approximately sevenfold increase in whole-body strength, with a persistent increase in muscle function, as enhanced muscle strength was observed in 12-mo-old mice. FHL1 induced a fiber type switch and increased the frequency of centralized myonuclei, which is consistent with hypertrophy. Overexpression of FHL1 also induced myotube hypertrophy in cultured C2C12 cells, as shown by increased myotube size, MHC accretion, and an increased protein/DNA ratio. These results, combined with the severe myopathy observed in individuals with FHL1 mutations, highlight the ability of FHL1 to regulate muscle mass.

Growth factors and increased muscle stretching or loading stimulate satellite cell proliferation and fusion with existing myofibers, leading to both increased myofiber size and centralization of myonuclei (Barton-Davis et al., 1999; Paul and Rosenthal, 2002). Hypertrophy is a multistep process and can occur because of expansion of the myofiber that is driven from within the fiber through maximized transcription and translation, resulting in increased protein synthesis. Enhanced myoblast differentiation and fusion also contribute to hypertrophy (Sandri, 2008). FHL1 may facilitate myofiber hypertrophy via enhanced myoblast fusion, as shown in C2C12 myoblasts and also through a mechanism within the fiber, as shown by the FHL1 transgenic muscle, in which the HSA promoter sequences

0–20 μm, >20–40 μm, and >40 μm, ±SEM (n > 300 myotubes from three experiments; n = 3; *, $P < 0.05$). (C) C2C12 myoblasts were cotransfected with various combinations of expression vectors as indicated, and with NFATc1-dependent (*pGL2-IL-2*) and Renilla luciferase reporters. Transfected myoblasts were maintained in growth media for 48 h and assayed for luciferase activity. Gal4DBD activity is represented by white bars and Gal4DBD-NFATc1 by gray bars. Error bars represent ± SEM ($n \geq 5$ experiments; *, $P < 0.05$). (D) Transfected myoblasts were differentiated for 48 h and assayed for luciferase activity (48 h; n = 4 experiments). (E) Gastrocnemius (GAS) lysates from wild-type (WT) or HA-FHL1 transgenic (TG) mice were immunoblotted for GATA-2 or β-tubulin (loading control). (F) GATA-2 protein expression levels in WT (white) versus TG (gray) gastrocnemius muscle was quantified using densitometry and standardized to the loading control. The bar graph represents the mean ± SEM (n = 5 mice per genotype; *, $P < 0.05$). (G) Transverse gastrocnemius muscle sections were costained with anti–GATA-2 (green), anti-vinculin (red; sarcolemma) antibodies, and To-Pro-3 iodide nuclear stain (blue), then imaged by confocal microscopy. Images were taken at the same intensity. Bars, 40 μm. (H) C2C12 cells were cotransfected with various combinations of expression vectors for Gal4DBD (white) or Gal4DBD-NFATc1 (gray) and either scrambled (control) or FHL1 siRNA oligonucleotides, as indicated, with NFATc1-dependent (*pGL2-IL-2*) and Renilla luciferase reporters. Assays were performed under growth conditions. Error bars represent ±SEM (n = 5 experiments; *, $P < 0.05$). (I) Luciferase assays performed in H were repeated under differentiation (48 h) conditions (n = 3 experiments; *, $P < 0.05$).

directed FHL1 expression in postmitotic myofibers. The observed increase in the frequency of centralized myonuclei in FHL1 transgenic skeletal muscle is consistent with enhanced fusion of activated satellite cells.

After dephosphorylation by calcineurin, NFATs translocate to the nucleus and activate or repress target genes (Horsley and Pavlath, 2002). Skeletal muscle electrical activity also promotes NFATc1 nuclear entry via calcineurin activation; however, NFATc1 can also shuttle in and out of the nucleus in the absence of calcineurin activation (Shen et al., 2006). Calcineurin signaling is proposed to regulate skeletal muscle fiber type switching (Chin et al., 1998; Naya et al., 2000). Early studies suggested calcineurin could induce skeletal muscle hypertrophy (Dunn et al., 1999; Semsarian et al., 1999b). However, transgenic mice expressing constitutively active calcineurin Aα (CnAα) in skeletal muscle do not exhibit hypertrophy (Naya et al., 2000), and gene-targeted deletion of specific calcineurin-isoforms (CnAα or CnAβ) does not lead to changes in myofiber diameter (Parsons et al., 2004). Calcineurin inhibition with high doses of CsA, which inhibits activation of most calcineurin isoforms, reduces overload-induced skeletal muscle hypertrophy. This suggests that global inhibition of all calcineurin activity may inhibit hypertrophy (Dunn et al., 1999). The calcineurin–NFAT pathway also promotes myoblast fusion to myotubes by enhancing IL-4 transcription (Fornaro et al., 2006).

We propose that FHL1 increases in muscle mass are a consequence of enhancing NFAT transcriptional activity. FHL1 promotes hyperfusion of C2C12 myoblasts, reversed by inhibition of the calcineurin–NFAT pathway. FHL1 transgenic muscle showed a muscle fiber type switch, which is consistent with calcineurin–NFAT activation, and increased expression of the calcineurin-responsive gene, GATA-2. NFATc2 is critical for secondary myogenesis, specifically the fusion of myoblasts with existing myotubes/myofibers (Horsley et al., 2001). NFATc2 knockout mice exhibit reduced muscle mass, a decrease in myofiber CSA, and reduced myonuclei number. Myoblast fusion occurs through an ordered series of events, which includes myoblast elongation, alignment, and fusion (Abmayr et al., 2003). We found that FHL1 promotes the hyper-elongation of myoblasts in an integrin-dependent manner (McGrath et al., 2003). Myoblast elongation is a critical step before myoblast fusion (Straube and Merdes, 2007; Fortier et al., 2008). The ability of FHL1 to promote myoblast elongation may contribute to the observed hyperfusion effect.

RBM occurs because of mutations in FHL1, which lead to muscle atrophy (Schessl et al., 2008). $FHL1^{C132F}$ and $FHL1^{H123Y}$ RBM mutants exhibited reduced NFATc1-mediated transcriptional activation, and unlike wild-type FHL1, do not induce hypertrophic myotubes. NFATc1 colocalized with mutant FHL1 to reducing body aggregates both in myotubes and in muscle from afflicted RBM individuals. When expressed with FHL1-RBM mutants, NFATc1 showed reduced nuclear translocation in response to calcineurin activation. These results suggest that mutant FHL1 contributes to RBM by reducing NFATc1-dependent transcription of genes that promote hypertrophy or regeneration. The reducing bodies that define RBM may arise from the accumulation of misfolded/unfolded FHL1 protein, (Meredith, 2005; Liewluck et al., 2007). Mutant FHL1 may bind NFATc1 with less affinity, as suggested by coimmunoprecipitation. Alternatively, the FHL1–NFATc1 complex is cosequestered to insoluble reducing body aggregates, making it less accessible for immunoprecipitation.

The $FHL1^{C132F}$ or $FHL1^{H123Y}$ mutations that cause RBM affect conserved, zinc-coordinating residues located in the second LIM domain. Two other myopathies in which FHL1 is mutated have been described. In one family, a W122S missense mutation was found in the second LIM domain, resulting in adult-onset X-linked dominant scapuloperoneal myopathy (Quinzii et al., 2008). Reducing bodies were not described in this paper. A third study describes a C224W missense mutation in the FHL1 fourth LIM domain and an isoleucine insertion between residue 127 and 128 in the second LIM domain. These mutations are both associated with a clinical presentation comprising adult-onset X-linked recessive disorder with hypertrophy of type 2 fibers, leading to pseudo-athleticism with atrophy of type 1 fibers, associated with postural atrophy and bent spine (XMPMA; Windpassinger et al., 2008). Whether these mutations also cause alteration in calcineurin–NFAT signaling is the subject of ongoing studies. These studies collectively describe seven distinct FHL1 mutations in sporadic and inherited myopathies, which lead to distinct phenotypes.

The calcineurin–NFAT pathway promotes muscle regeneration in some human myopathies (Sakuma et al., 2003). Calcineurin stimulation can ameliorate dystrophic pathology and myofiber atrophy, whereas a blockade of calcineurin signaling severely compromises muscle regeneration in *mdx* dystrophic mice (Chakkalakal et al., 2004). Genetic disruption of calcineurin improves the muscle pathology in δ-sarcoglycan–null mice, a mouse model of limb girdle muscular dystrophy-2F (Parsons et al., 2007), which implies a functional link between calcineurin–NFAT signaling and dystrophy/myopathy. We predict in RBM that the cosequestration of NFATc1 with mutant FHL1 to reducing bodies leads to loss of FHL1 function in enhancing muscle mass and impairs calcineurin–NFATc1 signaling.

In summary, we have identified FHL1 as a novel regulator of skeletal mass. FHL1 binds and regulates NFATc1 transcriptional activity, and this signaling complex is mislocalized into cytoplasmic aggregates in RBM. FHL1 may therefore represent a novel therapeutic target for increasing skeletal muscle mass in myopathies and conditions associated with muscle atrophy.

Materials and methods

Constructs

pCGN-FHL1 (human cDNA, GenBank/EMBL/DDBJ accession no. NM_001449), pGEX-5 × 1-FHL1, and pCGN-βgal (vector control) have been described previously (McGrath et al., 2003, 2006). pCMX and G5E1b-LUC vectors were gifts from R. Schule, (University of Freiburg, Freiburg, Germany). Mouse NFATc1 cDNA (GenBank/EMBL/DDBJ accession no. NM_016791) was PCR amplified from GFP-RV-DV-NFATc1 (plasmid 11101; Addgene; Table S2, available at http://www.jcb.org/cgi/content/full/jcb.200804077/DC1; Monticelli and Rao, 2002), and cloned into pCMX; pET-30a(+) (Novagen) and pEFBOS (provided by T. Wilson, the Walter and Eliza Hall Institute of Medical

Research, Melbourne, Australia). The *pGL2-IL-2* promoter–luciferase reporter (plasmid 10959; Addgene; Ichida and Finkel, 2001) and pHRLTK (renilla luciferase; Promega) were purchased. To generate pCGN-FHL1-C132F and H123Y, the HindIII to Pst1 fragment of wild-type FHL1 cDNA was excised from pCGN-FHL1 and exchanged for HindIII–Pst1 fragments containing C132F or H123Y mutations (Schessl et al., 2008). The pcDNA3.1 vector (HSA promoter) has been described previously (Corbett et al., 2001).

Reagents

Reagents were obtained as follows: C2C12 myoblasts (American Type Culture Collection); Optimem (Invitrogen); Lipofectamine 2000 (Invitrogen); fibronectin (Sigma-Aldrich); CsA, propidium iodide, and fibronectin (Sigma-Aldrich); glutathione–Sepharose 4B (GE Healthcare); dual-luciferase reporter assay system (Promega); and To-Pro-3 and the Quant-iT dsDNA assay kit (Invitrogen).

Antibodies

Primary antibodies used were: mouse anti-HA (Covance), β-tubulin (Invitrogen), pan-actin Ab-5 (Thermo Fischer Scientific), poly-histidine clone HIS-1, vinculin (Sigma-Aldrich), Pax-7 (R&D Systems), α-actinin (Sigma-Aldrich), rabbit anti-FHL1(McGrath et al., 2006), GATA-2 (H-116), NFATc1 (H-110; Santa Cruz Biotechnology, Inc.), myc (Cell Signaling Technology), c-myc (Bethyl Laboratories, Inc.), dystrophin (Abcam), goat anti-actin, MyoD (M318), Myf5 (C20), myogenin (F50 and M225; Santa Cruz Biotechnology, Inc.), GST (Amersham Biosciences), SC-71 (type 2A MHC), BF-F3 (type 2B MHC), BAF8 (type 1 MHC), and BF-35 (type 1, 2A, 2B MHCs) hybridomas (German Collection of Microorganisms and Cell Cultures). 6H1 (type 2X MHC) hybridoma supernatant was a gift from J. Hoh (University of Sydney, Sydney, Australia; Lucas et al., 2000). The sarcomeric MHC antibody (MF20) was obtained from the Developmental Studies Hybridoma Bank, developed under the auspices of the National Institutes of Health and maintained by the Department of Biological Sciences, University of Iowa (Bader et al., 1982). Secondary antibodies were as follows: anti–mouse, –rabbit, or –goat conjugated with HRP were obtained from Chemicon; FITC-conjugated anti–rabbit IgG was obtained from Chemicon; and all Alexa-conjugated secondary antibodies were from Invitrogen.

Generation of FHL1 transgenic mice

HA-tagged FHL1 (pCGN vector) was PCR amplified with flanking EcoRI sites and cloned into the pcDNA3.1+ vector containing an upstream HSA promoter (Brennan and Hardeman, 1993). The final 3.6-kb construct (Fig. 1 A) was excised by Nhe1–Nae1 digestion, purified, and microinjected into one-cell embryos, then implanted into pseudo-pregnant FVB/n mice. Positive founders were bred to FVB/n wild-type mice, and transgenic mice were selected by PCR analysis (Table S2). Animals were housed in a temperature-controlled room (19–22°C) with a 12:12-h light/dark cycle. Unless otherwise stated, all experiments were performed using 6- or 12-wk-old female transgenic mice and wild-type, sex-matched littermate controls, as indicated. Mice were humanely killed by CO_2 inhalation followed by cervical dislocation, according to the National Health and Medical Research Council guidelines (Monash University Animal Ethics no. BAM/2001/22).

Preparation of muscle lysates

The mouse gastrocnemius was dissected, minced, and homogenized on ice for 3 × 30 s (DIAX 900; Heidolph) in 10 times the weight/volume of 1% NP-40 Tris-Cl buffer, pH 8, then extracted for 1 h at 4°C. Lysates were centrifuged at 1,000 *g* for 30 s, and the total cell lysate obtained was stored at −80°C. Protein concentration was determined using a DC protein assay kit (Bio-Rad Laboratories). 20–100 µg of lysate was analyzed by SDS-PAGE and Western blotting.

Histological and immunofluorescence analysis of skeletal muscle

Longitudinal and transverse cryosections of gastrocnemius, EDL, soleus, and FDP mouse skeletal muscles were prepared, fixed, stained, viewed, and deconvolved where appropriate, as described previously (McGrath et al., 2006). To obtain polarized light microscopy images, fixed longitudinal sections from 12-wk-old male mice were viewed with a microscope (AX70; Olympus). When nuclear staining was required, sections were pretreated with 200 µg/ml RNase A (Sigma-Aldrich), and nuclei were detected by costaining with To-Pro-3 iodide (Invitrogen) or Dapi (Sigma-Aldrich) for 10 min. The total number of gastrocnemius muscle fibers with centralized nuclei or Pax-7–positive nuclei were counted in >500 fibers in at least three wild-type and transgenic mice using ImageJ image analysis software (version 1.34; National Institutes of Health). Alternatively, transverse FDP sections were placed on poly-L-lysine–precoated glass microscope slides, then air-dried, fixed, and stained with hematoxylin and eosin, and FDP fibers with centralized nuclei within the entire muscle section were counted.

Transverse human muscle sections were prepared, fixed, stained, and viewed as described previously (Schessl et al., 2008). Informed consent from human subjects was obtained (Institutional Review Board [IRB] approval 2002–6-2846 [the Children's Hospital of Philadelphia, Philadelphia, PA] and IRB approvals at the collaborating institutions).

Single myofibrils were isolated from mouse skeletal muscle, then fixed and stained as described previously (Knight and Trinick, 1982; McGrath et al., 2006). Myofibrils were viewed using a FV1000 laser scanning confocal microscope (Olympus). Widths of 20 myofibrils per mouse were measured using ImageJ software.

Muscle fiber diameter and area

CSA and minimum diameter were analyzed in gastrocnemius and FDP mouse skeletal muscle. Transverse 8-µm sections were prepared as described previously (McGrath et al., 2006) and viewed using a laser scanning confocal microscope (TCS NT; Leica). CSA (μm^2) and fiber diameter were calculated (gastrocnemius muscle had >500 fibers, all fibers in the FDP) from four to five mice per genotype for wild-type or FHL1 transgenic mice using the analySIS program (Olympus). Alternatively, fiber diameters were obtained from digital camera images of stained sections using the Image-Pro software (Media Cybernetics). Fiber diameter was determined by measuring the shortest axis for all fibers within a section to the nearest 10 µm, as described previously (Corbett et al., 2001).

Fiber type analysis

Transverse FDP mouse skeletal muscle sections were prepared, fixed, and stained for MHC isoforms, as described previously (Corbett et al., 2001; Nair-Shalliker et al., 2004). Sections were viewed using a microscope (BX50; Olympus) and captured using a Spot camera (V1.4.0) and Spot software (Diagnostic Instruments, Inc.). Images were collaged together using Photoshop (Adobe). The percentage of type 1, 2A, 2X, and 2B fibers were calculated in three to five wild-type and FHL1 transgenic mice.

Strength and fatigability test

The whole animal strength and fatigability test was performed on 12-wk- and 12-mo-old mice as described previously (Corbett et al., 2001; Joya et al., 2004).

Muscle contractile properties

EDL and soleus muscles were dissected tendon-to-tendon from anaesthetized mice (100 mg/kg BW ketamine and 10 mg/kg BW xylazine) for in vitro contractile measurements. Optimal muscle length (L_o) and maximum isometric tetanic force (P_o) were determined as described previously (Gregorevic et al., 2004). Stimulus conditions, lever arm control, and contractile data analysis were performed with DMC/DMA computer software (Aurora Scientific Inc.). Muscle fatigability was assessed and muscle CSA was determined as described previously (Gregorevic et al., 2004).

Growth, transient transfection, and immunofluorescence of C2C12 cells

C2C12 myoblasts were grown, transiently transfected with Lipofectamine 2000, and differentiated when indicated. Cells were then fixed, permeabilized, blocked, and stained with appropriate nuclear stains and/or antibodies, as described previously (McGrath et al., 2003, 2006; Cottle et al., 2007). When required, ionomycin diluted in DMSO was added to each well after 72 h in differentiation media, at a final concentration of 0.5 µM for 30 min. C2C12 cells were then immediately fixed and stained as described at the beginning of this paragraph. When required, 5 µM of CsA was added to C2C12 cells before and continuously during differentiation, as described previously (Musarò et al., 1999). To measure the myotube diameter, C2C12 cells were transfected as indicated and differentiated for 72 h. The maximum myotube diameter was measured in a total of >300 myotubes transfected with pCGN-FHL1 constructs from three experiments using ImageJ image analysis software (version 1.34).

For menadione-NBT staining, after immunofluorescence staining, cells were washed thoroughly with PBS, rinsed briefly with distilled H_2O (dH_2O), and stained with menadione-NBT (0.39 mg/ml menadione and 1 mg/ml NBT in gomori-Tris-HCl buffer, pH 7.4; Sigma-Aldrich) for 20 min at room temperature. Cells were washed with dH_2O and destained by brief washes in acetone (30%, 60%, 90%, 60%, and 30%) and rinsed again dH_2O. Samples were viewed using an AX70 microscope fitted with an

F-view II FW camera (Olympus). Images were taken using the analysis FIVE program (Olympus).

C2C12 differentiation

C2C12 myoblasts stably transfected with HA-βgal or HA-FHL1 have been described previously (McGrath et al., 2006). All experiments analyzing the differentiation of C2C12 myoblasts were performed as described previously (Cottle et al., 2007). In brief, 10^5 stably transfected myoblasts were plated onto fibronectin-coated coverslips (5 µg/ml) and induced to differentiate to myotubes for 0–96 h. At 24-h intervals after the induction of differentiation, cells were either fixed and stained for immunofluorescence studies, or lysates were prepared and Western blot analyses performed. For immunofluorescence experiments, cells were costained with anti-myogenin (M225; 1:100) and anti-MHC (MF20; 1:100) antibodies. To detect nuclei, cells were pretreated with 200 µg/ml RNase A for 1 h and stained with 25 µg/well propidium iodide for 5 min. Cells were imaged using confocal microscopy, and several well-defined parameters of myoblast differentiation were examined, including: (A) the proportion of total nuclei positive for myogenin staining, (B) the differentiation index (proportion of nuclei localized within MHC-positive myotubes), and (C) the fusion index (mean number of nuclei per MHC-positive myotube; Sabourin et al., 1999). Each experiment was performed in triplicate, and for all cell counts, a minimum of four random fields were scanned for each slide to ensure that ≥100 cells were scored for each replicate. Cells counts were quantified using ImageJ software (version 1.34; Abramoff et al., 2004). For Western blot analyses, Triton X-100–soluble lysates were prepared, protein concentration was measured using a D_C protein assay reagent (Bio-Rad Laboratories), and 25-µg lysates were immunoblotted with MyoD (1:100), Myf5 (1:100), myogenin (F50; 1:500), MHC (MF20; 1:500), and β-tubulin (1:5,000) antibodies as described previously (Cottle et al., 2007).

Protein/DNA ratio

The method for measurement of the protein/DNA ratio of C2C12 myotubes was adapted from De Arcangelis et al. (2005) and Nakamura et al. (2000). In brief, 10^5 C2C12 myoblasts stably expressing HA-βgal or HA-FHL1, described previously (McGrath et al., 2006), were plated in a 6-well dish and induced to differentiate for 96 h. Cells were rinsed in cold PBS and lysed using 0.05% Triton X-100 in TE5N buffer (10 mM Tris-HCl, pH 8, 0.1 mM EDTA, 0.5 M NaCl, and a protease inhibitor tablet; Roche). Lysates were cleared by low-speed centrifugation (2,000 rpm, 5 min). Protein concentration was measured using a D_C protein assay reagent. DNA concentration was determined using a Quant-iT dsDNA assay kit (Invitrogen) and measured using Fluostar Optima plate reader (BMG Labtech).

In vitro direct protein interaction

Escherichia coli strain BL21 DE3 Gold Codon Plus RP (Agilent Technologies) was cotransformed with pGEX-5 × 1(GST-tag), pGEX-5 × 1-FHL1, or, pGEX-5 × 1-GATA-2 together with pET-30a(+)(His-tag) or pET-30a(+)-NFATc1. Recombinant protein production was induced, and direct protein interaction and immunoblotting were performed as described previously (Cottle et al., 2007).

GST pull-down in mouse skeletal muscle lysate

Recombinant, bacterially expressed GST and GST-FHL1 protein was produced and purified as described previously (Cottle et al., 2007). Muscle lysates were prepared from wild-type FVB/n mice, as described in "Preparation of muscle lysates," in 1% NP-40 Hepes lysis buffer, then precleared for 1 h with glutathione–Sepharose 4B beads. GST pull-down and immunoblotting were performed as described previously (Cottle et al., 2007).

Coimmunoprecipitation from C2C12 myoblasts

C2C12 myoblasts maintained in 100-mm dishes were cotransfected with 24 µg (pCGN constructs) and 6 µg (pEFBOS constructs) of DNA using 30 µl Lipofectamine 2000 according to the manufacturer's instructions. Coimmunoprecipitation was performed with 3 µl of myc antibody (Cell Signaling Technology), as described previously (McGrath et al., 2006).

Luciferase assays

Luciferase assays were performed with *pGL2-IL-2* promoter–luciferase reporter (1 µg) using Lipofectamine 2000 as described previously (Cottle et al., 2007). siRNA oligonucleotides specific for mouse FHL1 cDNA (GenBank/EMBL/DDBJ accession no. NM_010211; siRNA FHL1) or scrambled control (siRNA control; QIAGEN; Table S2) were previously validated for use in C2C12 myoblasts (McGrath et al., 2006).

Image and statistical analysis

All microscopy was performed at Monash Microimaging at Monash University, Australia. All samples for microscopy were mounted in SlowFade reagent (Invitrogen) and viewed at room temperature. Confocal microscopy was performed using a confocal laser scanning microscope (TCS/NT; Leica) on a DMRBE upright microscope. Leica Confocal Software (LCS version 2.5; Leica) was used for confocal image acquisition. Fluorescence and light microscopy was performed using a microscope (AX70 Provis; Olympus) fitted with either a charge-coupled device (color; DP70; Olympus) or FVII monochrome (black and white; Olympus) camera. AnalySiS software was used for image capture and analysis.

Western blot films were scanned and band signal intensities were determined using a Gel-Pro Analyzer (version 3.1; Media Cybernetics). Densitometry values were expressed as a fold difference relative to the control, standardized to corresponding total actin/β-tubulin values. All results are presented as the mean ± SE (SEM). Statistical analysis was performed using the unpaired student's *t* test unless stated otherwise. p-values of <0.05 were considered significant.

Online supplemental material

Fig. S1 shows the normal morphology of the sarcomere and the increased myofibril width in FHL1 transgenic mice. Fig. S2 shows hypertrophy of type 2B fibers of the EDL in FHL1 transgenic mice. Fig. S3 shows knockdown of endogenous FHL1 in C2C12 cells using FHL1 siRNA oligonucleotides. Table S1 shows the contractile data from EDL muscles of FHL1 transgenic and wild-type mice. Table S2 shows the sequences of all oligonucleotides used. Online supplemental material is available at http://www.jcb.org/cgi/content/full/jcb.200804077/DC1.

We thank Gordon Lynch and David Plant for their advice on the whole muscle contractile measurements, and we also thank Monash MicroImaging.

This work was funded in part by Australian National Health and Medical Research Project grants 436637 (to C. Mitchell and E. Hardeman), 321701 (to E. Hardeman), and 321705 (to E. Hardeman and A. Kee). B. Cowling was supported by a Monash Graduate Scholarship. M.-A. Nguyen is supported by a University of Sydney Postgraduate Award.

Submitted: 15 April 2008
Accepted: 14 November 2008

References

Abbott, K.L., B.B. Friday, D. Thaloor, T.J. Murphy, and G.K. Pavlath. 1998. Activation and cellular localization of the cyclosporine A-sensitive transcription factor NF-AT in skeletal muscle cells. *Mol. Biol. Cell.* 9:2905–2916.

Abmayr, S.M., L. Balagopalan, B.J. Galletta, and S.J. Hong. 2003. Cell and molecular biology of myoblast fusion. *Int. Rev. Cytol.* 225:33–89.

Abramoff, M.D., P.J. Magelhaes, and S.J. Ram. 2004. Image processing with ImageJ. *Biophotonics International.* 11:36–42.

Adams, G.R. 2006. Satellite cell proliferation and skeletal muscle hypertrophy. *Appl. Physiol. Nutr. Metab.* 31:782–790.

Bader, D., T. Masaki, and D.A. Fischman. 1982. Immunochemical analysis of myosin heavy chain during avian myogenesis in vivo and in vitro. *J. Cell Biol.* 95:763–770.

Barton-Davis, E.R., D.I. Shoturma, and H.L. Sweeney. 1999. Contribution of satellite cells to IGF-I induced hypertrophy of skeletal muscle. *Acta Physiol. Scand.* 167:301–305.

Boonyarom, O., and K. Inui. 2006. Atrophy and hypertrophy of skeletal muscles: structural and functional aspects. *Acta Physiol (Oxf.).* 188:77–89.

Brennan, K.J., and E.C. Hardeman. 1993. Quantitative analysis of the human alpha-skeletal actin gene in transgenic mice. *J. Biol. Chem.* 268:719–725.

Brooke, M.H., and H.E. Neville. 1972. Reducing body myopathy. *Neurology.* 22:829–840.

Chakkalakal, J.V., M.A. Harrison, S. Carbonetto, E. Chin, R.N. Michel, and B.J. Jasmin. 2004. Stimulation of calcineurin signaling attenuates the dystrophic pathology in mdx mice. *Hum. Mol. Genet.* 13:379–388.

Chin, E.R., E.N. Olson, J.A. Richardson, Q. Yang, C. Humphries, J.M. Shelton, H. Wu, W. Zhu, R. Bassel-Duby, and R.S. Williams. 1998. A calcineurin-dependent transcriptional pathway controls skeletal muscle fiber type. *Genes Dev.* 12:2499–2509.

Cole, F., T.M. Fasy, S.S. Rao, M.A. de Peralta, and D.S. Kohtz. 1993. Growth factors that repress myoblast differentiation sustain phosphorylation of a specific site on histone H1. *J. Biol. Chem.* 268:1580–1585.

Corbett, M.A., C.S. Robinson, G.F. Dunglison, N. Yang, J.E. Joya, A.W. Stewart, C. Schnell, P.W. Gunning, K.N. North, and E.C. Hardeman. 2001. A mutation in alpha-tropomyosin(slow) affects muscle strength, maturation and hypertrophy in a mouse model for nemaline myopathy. *Hum. Mol. Genet.* 10:317–328.

Cottle, D.L., M.J. McGrath, B.S. Cowling, I.D. Coghill, S. Brown, and C.A. Mitchell. 2007. FHL3 binds MyoD and negatively regulates myotube formation. *J. Cell Sci.* 120:1423–1435.

Cox, R.D., I. Garner, and M.E. Buckingham. 1990. Transcriptional regulation of actin and myosin genes during differentiation of a mouse muscle cell line. *Differentiation.* 43:183–191.

De Arcangelis, V., D. Coletti, M. Canato, M. Molinaro, S. Adamo, C. Reggiani, and F. Naro. 2005. Hypertrophy and transcriptional regulation induced in myogenic cell line L6-C5 by an increase of extracellular calcium. *J. Cell. Physiol.* 202:787–795.

Delling, U., J. Tureckova, H.W. Lim, L.J. De Windt, P. Rotwein, and J.D. Molkentin. 2000. A calcineurin-NFATc3-dependent pathway regulates skeletal muscle differentiation and slow myosin heavy-chain expression. *Mol. Cell. Biol.* 20:6600–6611.

Dunn, S.E., J.L. Burns, and R.N. Michel. 1999. Calcineurin is required for skeletal muscle hypertrophy. *J. Biol. Chem.* 274:21908–21912.

Erbay, E., I.H. Park, P.D. Nuzzi, C.J. Schoenherr, and J. Chen. 2003. IGF-II transcription in skeletal myogenesis is controlled by mTOR and nutrients. *J. Cell Biol.* 163:931–936.

Figarella-Branger, D., G.A. Putzu, C. Bouvier-Labit, J. Pouget, D. Chateau, M. Fardeau, and J.F. Pellissier. 1999. Adult onset reducing body myopathy. *Neuromuscul. Disord.* 9:580–586.

Fornaro, M., P.M. Burch, W. Yang, L. Zhang, C.E. Hamilton, J.H. Kim, B.G. Neel, and A.M. Bennett. 2006. SHP-2 activates signaling of the nuclear factor of activated T cells to promote skeletal muscle growth. *J. Cell Biol.* 175:87–97.

Fortier, M., F. Comunale, J. Kucharczak, A. Blangy, S. Charrasse, and C. Gauthier-Rouviere. 2008. RhoE controls myoblast alignment prior fusion through RhoA and ROCK. *Cell Death Differ.* 15:1221–1231.

Friday, B.B., V. Horsley, and G.K. Pavlath. 2000. Calcineurin activity is required for the initiation of skeletal muscle differentiation. *J. Cell Biol.* 149:657–666.

Furmanczyk, P.S., and L.S. Quinn. 2003. Interleukin-15 increases myosin accretion in human skeletal myogenic cultures. *Cell Biol. Int.* 27:845–851.

Gregorevic, P., D.R. Plant, and G.S. Lynch. 2004. Administration of insulin-like growth factor-I improves fatigue resistance of skeletal muscles from dystrophic mdx mice. *Muscle Nerve.* 30:295–304.

Gunning, P., E. Hardeman, R. Wade, P. Ponte, W. Bains, H.M. Blau, and L. Kedes. 1987. Differential patterns of transcript accumulation during human myogenesis. *Mol. Cell. Biol.* 7:4100–4114.

Gunther, T., C. Poli, J.M. Muller, P. Catala-Lehnen, T. Schinke, N. Yin, S. Vomstein, M. Amling, and R. Schule. 2005. Fhl2 deficiency results in osteopenia due to decreased activity of osteoblasts. *EMBO J.* 24:3049–3056.

Horsley, V., and G.K. Pavlath. 2002. NFAT: ubiquitous regulator of cell differentiation and adaptation. *J. Cell Biol.* 156:771–774.

Horsley, V., B.B. Friday, S. Matteson, K.M. Kegley, J. Gephart, and G.K. Pavlath. 2001. Regulation of the growth of multinucleated muscle cells by an NFATC2-dependent pathway. *J. Cell Biol.* 153:329–338.

Ichida, M., and T. Finkel. 2001. Ras regulates NFAT3 activity in cardiac myocytes. *J. Biol. Chem.* 276:3524–3530.

Johannessen, M., S. Moller, T. Hansen, U. Moens, and M. Van Ghelue. 2006. The multifunctional roles of the four-and-a-half-LIM only protein FHL2. *Cell. Mol. Life Sci.* 63:268–284.

Joya, J.E., A.J. Kee, V. Nair-Shalliker, M. Ghoddusi, M.A. Nguyen, P. Luther, and E.C. Hardeman. 2004. Muscle weakness in a mouse model of nemaline myopathy can be reversed with exercise and reveals a novel myofiber repair mechanism. *Hum. Mol. Genet.* 13:2633–2645.

Kegley, K.M., J. Gephart, G.L. Warren, and G.K. Pavlath. 2001. Altered primary myogenesis in NFATC3(−/−) mice leads to decreased muscle size in the adult. *Dev. Biol.* 232:115–126.

Kiyomoto, B.H., N. Murakami, Y. Kobayashi, K. Nihei, T. Tanaka, K. Takeshita, and I. Nonaka. 1995. Fatal reducing body myopathy. Ultrastructural and immunohistochemical observations. *J. Neurol. Sci.* 128:58–65.

Knight, P.J., and J.A. Trinick. 1982. Preparation of myofibrils. *Methods Enzymol.* 85 Pt. B:9–12.

Liewluck, T., Y.K. Hayashi, M. Ohsawa, R. Kurokawa, M. Fujita, S. Noguchi, I. Nonaka, and I. Nishino. 2007. Unfolded protein response and aggresome formation in hereditary reducing-body myopathy. *Muscle Nerve.* 35:322–326.

Loughna, P.T., P. Mason, S. Bayol, and C. Brownson. 2000. The LIM-domain protein FHL1 (SLIM 1) exhibits functional regulation in skeletal muscle. *Mol. Cell Biol. Res. Commun.* 3:136–140.

Lucas, C.A., L.H. Kang, and J.F. Hoh. 2000. Monospecific antibodies against the three mammalian fast limb myosin heavy chains. *Biochem. Biophys. Res. Commun.* 272:303–308.

Marshall, A., M.S. Salerno, M. Thomas, T. Davies, C. Berry, K. Dyer, J. Bracegirdle, T. Watson, M. Dziadek, R. Kambadur, et al. 2008. Mighty is a novel promyogenic factor in skeletal myogenesis. *Exp. Cell Res.* 314: 1013–1029.

McGrath, M.J., C.A. Mitchell, I.D. Coghill, P.A. Robinson, and S. Brown. 2003. Skeletal muscle LIM protein 1 (SLIM1/FHL1) induces alpha 5 beta 1-integrin-dependent myocyte elongation. *Am. J. Physiol. Cell Physiol.* 285: C1513–C1526.

McGrath, M.J., D.L. Cottle, M.A. Nguyen, J.M. Dyson, I.D. Coghill, P.A. Robinson, M. Holdsworth, B.S. Cowling, E.C. Hardeman, C.A. Mitchell, and S. Brown. 2006. Four and a half LIM protein 1 binds myosin-binding protein C and regulates myosin filament formation and sarcomere assembly. *J. Biol. Chem.* 281:7666–7683.

Meredith, S.C. 2005. Protein denaturation and aggregation: Cellular responses to denatured and aggregated proteins. *Ann. N. Y. Acad. Sci.* 1066:181–221.

Miniou, P., D. Tiziano, T. Frugier, N. Roblot, M. Le Meur, and J. Melki. 1999. Gene targeting restricted to mouse striated muscle lineage. *Nucleic Acids Res.* 27:e27.

Monticelli, S., and A. Rao. 2002. NFAT1 and NFAT2 are positive regulators of IL-4 gene transcription. *Eur. J. Immunol.* 32:2971–2978.

Morgan, M.J., and A.J. Madgwick. 1999. The LIM proteins FHL1 and FHL3 are expressed differently in skeletal muscle. *Biochem. Biophys. Res. Commun.* 255:245–250.

Morgan, M.J., A.J. Madgwick, B. Charleston, J.M. Pell, and P.T. Loughna. 1995. The developmental regulation of a novel muscle LIM-protein. *Biochem. Biophys. Res. Commun.* 212:840–846.

Musarò, A., and N. Rosenthal. 1999. Maturation of the myogenic program is induced by postmitotic expression of insulin-like growth factor I. *Mol. Cell. Biol.* 19:3115–3124.

Musarò, A., K.J. McCullagh, F.J. Naya, E.N. Olson, and N. Rosenthal. 1999. IGF-1 induces skeletal myocyte hypertrophy through calcineurin in association with GATA-2 and NF-ATc1. *Nature.* 400:581–585.

Nair-Shalliker, V., A.J. Kee, J.E. Joya, C.A. Lucas, J.F. Hoh, and E.C. Hardeman. 2004. Myofiber adaptational response to exercise in a mouse model of nemaline myopathy. *Muscle Nerve.* 30:470–480.

Nakamura, Y., T. Haneda, J. Osaki, S. Miyata, and K. Kikuchi. 2000. Hypertrophic growth of cultured neonatal rat heart cells mediated by vasopressin V(1A) receptor. *Eur. J. Pharmacol.* 391:39–48.

Naya, F.J., B. Mercer, J. Shelton, J.A. Richardson, R.S. Williams, and E.N. Olson. 2000. Stimulation of slow skeletal muscle fiber gene expression by calcineurin in vivo. *J. Biol. Chem.* 275:4545–4548.

O'Connor, R.S., and G.K. Pavlath. 2007. Point:Counterpoint: Satellite cell addition is/is not obligatory for skeletal muscle hypertrophy. *J. Appl. Physiol.* 103:1099–1100.

O'Connor, R.S., S.T. Mills, K.A. Jones, S.N. Ho, and G.K. Pavlath. 2007. A combinatorial role for NFAT5 in both myoblast migration and differentiation during skeletal muscle myogenesis. *J. Cell Sci.* 120:149–159.

Palmer, S., N. Groves, A. Schindeler, T. Yeoh, C. Biben, C.C. Wang, D.B. Sparrow, L. Barnett, N.A. Jenkins, N.G. Copeland, et al. 2001. The small muscle-specific protein Csl modifies cell shape and promotes myocyte fusion in an Insulin-like growth factor 1-dependent manner. *J. Cell Biol.* 153:985–998.

Parsons, S.A., D.P. Millay, B.J. Wilkins, O.F. Bueno, G.L. Tsika, J.R. Neilson, C.M. Liberatore, K.E. Yutzey, G.R. Crabtree, R.W. Tsika, and J.D. Molkentin. 2004. Genetic loss of calcineurin blocks mechanical overload-induced skeletal muscle fiber type switching but not hypertrophy. *J. Biol. Chem.* 279:26192–26200.

Parsons, S.A., D.P. Millay, M.A. Sargent, F.J. Naya, E.M. McNally, H.L. Sweeney, and J.D. Molkentin. 2007. Genetic disruption of calcineurin improves skeletal muscle pathology and cardiac disease in a mouse model of limb-girdle muscular dystrophy. *J. Biol. Chem.* 282:10068–10078.

Patel, K., and F. Muntoni. 2004. Inducing muscle hypertrophy as a therapeutic strategy for muscular dystrophies. 122nd ENMC International Workshop, Naarden, The Netherlands, 28-30 November 2003. *Neuromuscul. Disord.* 14:519–525.

Paul, A.C., and N. Rosenthal. 2002. Different modes of hypertrophy in skeletal muscle fibers. *J. Cell Biol.* 156:751–760.

Pisconti, A., S. Brunelli, M. Di Padova, C. De Palma, D. Deponti, S. Baesso, V. Sartorelli, G. Cossu, and E. Clementi. 2006. Follistatin induction by nitric oxide through cyclic GMP: a tightly regulated signaling pathway that controls myoblast fusion. *J. Cell Biol.* 172:233–244.

Quinzii, C.M., T.H. Vu, K.C. Min, K. Tanji, S. Barral, R.P. Grewal, A. Kattah, P. Camano, D. Otaegui, T. Kunimatsu, et al. 2008. X-linked dominant scapuloperoneal myopathy is due to a mutation in the gene encoding four-and-a-half-LIM protein 1. *Am. J. Hum. Genet.* 82:208–213.

Rommel, C., S.C. Bodine, B.A. Clarke, R. Rossman, L. Nunez, T.N. Stitt, G.D. Yancopoulos, and D.J. Glass. 2001. Mediation of IGF-1-induced skeletal myotube hypertrophy by PI(3)K/Akt/mTOR and PI(3)K/Akt/GSK3 pathways. *Nat. Cell Biol.* 3:1009–1013.

Rosenblatt, J.D., and R.I. Woods. 1992. Hypertrophy of rat extensor digitorum longus muscle injected with bupivacaine. A sequential histochemical, immunohistochemical, histological and morphometric study. *J. Anat.* 181: 11–27.

Sabourin, L.A., A. Girgis-Gabardo, P. Seale, A. Asakura, and M.A. Rudnicki. 1999. Reduced differentiation potential of primary MyoD−/− myogenic cells derived from adult skeletal muscle. *J. Cell Biol.* 144:631–643.

Sakuma, K., J. Nishikawa, R. Nakao, K. Watanabe, T. Totsuka, H. Nakano, M. Sano, and M. Yasuhara. 2003. Calcineurin is a potent regulator for skeletal muscle regeneration by association with NFATc1 and GATA-2. *Acta Neuropathol.* 105:271–280.

Sandri, M. 2008. Signaling in muscle atrophy and hypertrophy. *Physiology (Bethesda).* 23:160–170.

Sanger, J.W., P. Chowrashi, N.C. Shaner, S. Spalthoff, J. Wang, N.L. Freeman, and J.M. Sanger. 2002. Myofibrillogenesis in skeletal muscle cells. *Clin. Orthop. Relat. Res.*:S153–S162.

Schessl, J., Y. Zou, M.J. McGrath, B.S. Cowling, B. Maiti, S.S. Chin, C. Sewry, R. Battini, Y. Hu, D.L. Cottle, et al. 2008. Proteomic identification of FHL1 as the protein mutated in human reducing body myopathy. *J. Clin. Invest.* 118:904–912.

Semsarian, C., P. Sutrave, D.R. Richmond, and R.M. Graham. 1999a. Insulin-like growth factor (IGF-I) induces myotube hypertrophy associated with an increase in anaerobic glycolysis in a clonal skeletal-muscle cell model. *Biochem. J.* 339:443–451.

Semsarian, C., M.J. Wu, Y.K. Ju, T. Marciniec, T. Yeoh, D.G. Allen, R.P. Harvey, and R.M. Graham. 1999b. Skeletal muscle hypertrophy is mediated by a Ca2+-dependent calcineurin signalling pathway. *Nature.* 400:576–581.

Shen, T., Y. Liu, Z. Cseresnyes, A. Hawkins, W.R. Randall, and M.F. Schneider. 2006. Activity- and calcineurin-independent nuclear shuttling of NFATc1, but not NFATc3, in adult skeletal muscle fibers. *Mol. Biol. Cell.* 17:1570–1582.

Shen, X., J.M. Collier, M. Hlaing, L. Zhang, E.H. Delshad, J. Bristow, and H.S. Bernstein. 2003. Genome-wide examination of myoblast cell cycle withdrawal during differentiation. *Dev. Dyn.* 226:128–138.

St-Pierre, S.J., J.V. Chakkalakal, S.M. Kolodziejczyk, J.C. Knudson, B.J. Jasmin, and L.A. Megeney. 2004. Glucocorticoid treatment alleviates dystrophic myofiber pathology by activation of the calcineurin/NF-AT pathway. *FASEB J.* 18:1937–1939.

Stevenson, E.J., A. Koncarevic, P.G. Giresi, R.W. Jackman, and S.C. Kandarian. 2005. Transcriptional profile of a myotube starvation model of atrophy. *J. Appl. Physiol.* 98:1396–1406.

Straube, A., and A. Merdes. 2007. EB3 regulates microtubule dynamics at the cell cortex and is required for myoblast elongation and fusion. *Curr. Biol.* 17:1318–1325.

Tinsley, J.M., A.C. Potter, S.R. Phelps, R. Fisher, J.I. Trickett, and K.E. Davies. 1996. Amelioration of the dystrophic phenotype of mdx mice using a truncated utrophin transgene. *Nature.* 384:349–353.

Windpassinger, C., B. Schoser, V. Straub, S. Hochmeister, A. Noor, B. Lohberger, N. Farra, E. Petek, T. Schwarzbraun, L. Ofner, et al. 2008. An X-linked myopathy with postural muscle atrophy and generalized hypertrophy, termed XMPMA, is caused by mutations in FHL1. *Am. J. Hum. Genet.* 82:88–99.

Yoshida, N., S. Yoshida, K. Koishi, K. Masuda, and Y. Nabeshima. 1998. Cell heterogeneity upon myogenic differentiation: down-regulation of MyoD and Myf-5 generates 'reserve cells'. *J. Cell Sci.* 111:769–779.